KfK 4445
November 1989

Accident Consequence Assessments with Different Atmospheric Dispersion Models

A Benchmark Study

H.-J. Panitz
Institut für Neutronenphysik und Reaktortechnik
Projektgruppe LWR-Sicherheit

Kernforschungszentrum Karlsruhe

KERNFORSCHUNGSZENTRUM KARLSRUHE
Institut für Neutronenphysik und Reaktortechnik
Projektgruppe LWR-Sicherheit

KfK 4445

ACCIDENT CONSEQUENCE ASSESSMENTS WITH DIFFERENT ATMOSPHERIC DISPERSION MODELS - A BENCHMARK STUDY -

H.-J. Panitz [1]

[1] present affiliation:
Institut für Meteorologie und Klimaforschung

This work has been performed with support of the
Commission of the European Communities
Radiation Protection Programme
Contract No. BI6/F/128/D

Kernforschungszentrum Karlsruhe GmbH, Karlsruhe

Kernforschungszentrum Karlsruhe GmbH
Postfach 3640, 7500 Karlsruhe 1

ISSN 0303-4003

Abstract

An essential aim of the improvements of the new program system **UFOMOD** for **Accident Consequence Assessments** (ACAs) was to substitute the straight-line Gaussian plume model conventionally used in ACA models by more realistic atmospheric dispersion models. To identify improved models which can be applied in ACA codes and to quantify the implications of different dispersion models on the results of an ACA, probabilistic comparative calculations with different atmospheric dispersion models have been performed. The study showed that there are trajectory models available which can be applied in ACAs and that they provide more realistic results of ACAs than straight-line Gaussian models. This led to a completely novel concept of atmospheric dispersion modelling in which two different distance ranges of validity are distinguished: the near range of some ten kilometres distance and the adjacent far range which are assigned to respective trajectory models.

Unfallfolgenabschätzungen mit verschiedenen atmosphärischen Ausbreitungsmodellen - eine vergleichende Untersuchung -

ZUSAMMENFASSUNG

Ein wesentliches Ziel der Verbesserungen des neuen Programmsystems **UFOMOD** zur Abschätzung der Folgen kerntechnischer Unfälle war es, das geradlinige Gauß'sche Fahnenmodell, das bisher üblicherweise in Unfallfolgenmodellen benutzt wurde, durch realistischere atmosphärische Ausbreitungsmodelle zu ersetzen. Um verbesserte Modelle, die in Unfallfolgenabschätzungen eingesetzt werden können, zu identifizieren, und um die Auswirkungen, die unterschiedliche Modellierungen der atmosphärischen Ausbreitung auf die Abschätzungen haben können, zu quantifizieren, wurden probabilistische Vergleichsrechnungen mit verschiedenen Ausbreitungsmodellen durchgeführt. Die Studie zeigte, daß Trajektorienmodelle verfügbar sind, die in Unfallfolgenmodellen verwendet werden können, und daß sie realistischere Ergebnisse liefern als das geradlinige Gaußmodell. Dies führte zu einer für Unfallfolgenabschätzungen völlig neuen Konzeption der Modellierung der atmosphärischen Ausbreitung, wobei zwischen zwei Entfernungsbereichen unterschieden wurde: dem Nahbereich bis zu einigen zehn Kilometern Quelldistanz und dem sich anschließenden Fernbereich. Beiden Entfernungsbereichen wurden entsprechende Trajektorienmodelle zugeordnet.

Table of Contents

List of Illustrations

List of Tables

1. INTRODUCTION

Off-site **Accident Consequence Assessments (ACAs)** estimate the spectrum of radiological consequences after accidental releases of radionuclides from nuclear installations into the atmosphere [1], [2]. Atmospheric dispersion, deposition, and environmental transfer lead to spatial and temporal distributions of activity in the affected environment. The resulting off-site consequences which need to be evaluated in an ACA can be divided into two broad categories: first, there are the health effects in the exposed population and its descendants, and second, there is the impact of countermeasures which may be taken to reduce exposure and thus the health implications in the population. Since the occurrence of accidents cannot be pre-determined, the consequences following such postulated accidents can only be estimated probabilistically.

Accidental releases into the atmosphere are the most severe ones in terms of the radiological consequences. Therefore, modelling the atmospheric dispersion and deposition is of essential importance in an ACA. Once the material is released, the particles and gases form a plume which is transported along the wind direction and expands horizontally and vertically due to diffusion conducted by turbulent eddies in the atmosphere (Figure 1).

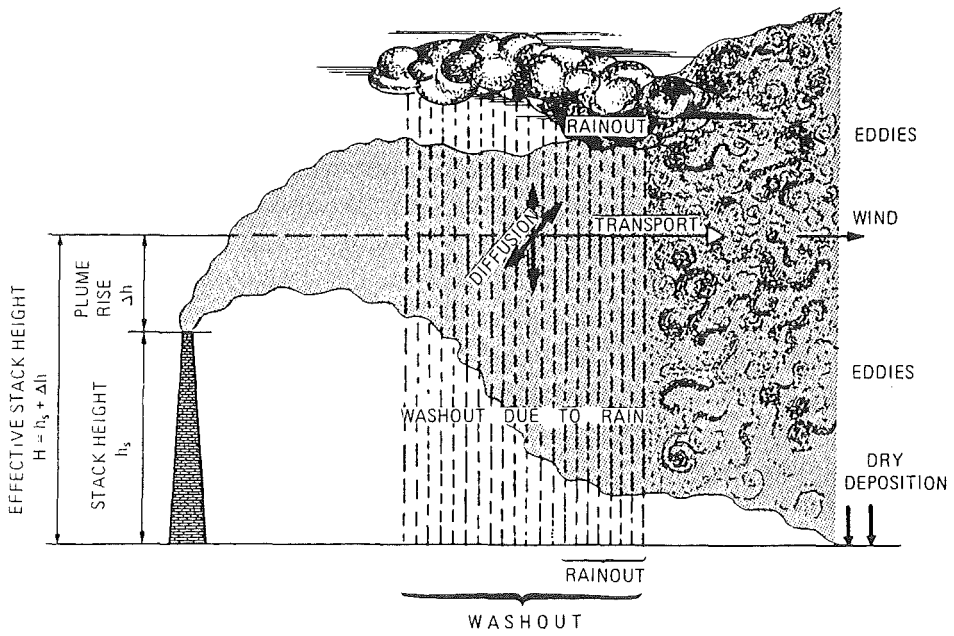

Figure 1. Behaviour of radionuclides released to the atmosphere (from [3])

During the dispersion the material may be removed from the plume by several mechanisms. Gravitational settling and contact with the ground, vegetation and structure in urban areas are referred to as dry deposition. Wet deposition may result from precipitation formation processes within the cloud, leading to removal by rainout, or from interaction between falling rain drops and the dispersing material, referred to as washout. Additionally, radioactive decay reduces the activity in the plume. Depending on the

release characteristics special features may have influence on the dispersion and deposition, for example the effect of plume rise due to the buoyancy or momentum of the released activity and the behaviour of plumes released into building wakes.

To simulate the very complex processes whereby material is dispersed in and deposited from the atmosphere and to calculate the resulting distributions of activity concentrations in the air and on the ground a large number of models of different physical complexity has been developed. The well-known straight-line Gaussian plume model assumes that the concentration C(x,y,z) across the plume can be described by a bi-Gaussian distribution [4]. Due to its simplicity the straight-line Gaussian model is the one most commonly used in practical applications of atmospheric dispersion modelling. Also in most of the computer programs developed for ACAs in the last ten years, e.g. CRAC [5], CRAC2 [6], MARC [7], MACCS [8], and UFOMOD [2], this model has been implemented to describe the atmospheric dispersion and deposition.

The application of the straight-line Gaussian model is restricted to only a limited range of atmospheric and environmental conditions, because basic assumptions for its derivation are that the terrain over which the material is dispersing is uniform and that the atmospheric flow- and turbulence fields are constant in space and time. Recently, the model has been improved to consider temporal, e.g. hourly, variations of wind speed, precipitation intensity, and dispersion category [1]. However, the model does not allow for changes of wind direction during the release and during the subsequent dispersion of the released material through the atmosphere. Also extreme weather conditions with weak wind, wind shear and inversion cannot be considered.

In the last years a large number of dispersion models has been developed which describe the physical conditions in the atmosphere more realistically. Trajectory plume and trajectory puff models also assume Gaussian profiles of concentrations across the plume or puff. In contrast to the straight-line Gaussian model they are able to consider variations of the meteorological fields. Alternatives to the Gaussian-type models provide the Eulerian gradient transport- and the Lagrangian statistical models. These more complex models are able to take into account the three-dimensional instationary and inhomogeneous atmospheric conditions. The Eulerian (K-) model solves the diffusion-advection equation numerically on a grid at defined spatial points. The Lagrangian model simulates the atmospheric dispersion by tracking the trajectories of a large amount of individual particles taking into account the turbulent, which means random or stochastic, nature of wind speed by statistical methods. A detailed description of different types of atmospheric dispersion models can be found in [9].

The consequences of a postulated release of radioactive material will vary considerably with the conditions pertaining at the time, in particular with the prevailing meteorological conditions. Therefore, it is necessary to repeat the atmospheric dispersion calculation with a large amount of weather sequences representing different meteorological situations to predict the full distribution of consequences which may occur following an accidental release. Because of this a balance must be found between the need to obtain an accurate and reliable prediction of concentrations and the need to reduce computer time, e.g. the use of a relatively simple model. The availability of meteorological data also effects the applicability of a dispersion model in an ACA code, as in general the more complex the models are the larger is the amount of data they require. Therefore, an

atmospheric dispersion model as a part of an ACA program system has to fulfill the following, somewhat contradictory, demands:

- atmospheric and environmental conditions should be considered as realistic as possible to get reliable predictions of the distributions of concentrations,
- the required computer time must be reasonable because a lot of different weather sequences has to be taken into account,
- the meteorological data needed should be derived from routine observations which are recorded and reported continuously from meteorological stations with a rather high frequency (e.g. hourly).

Up to now there is a lack of quantitative and qualitative studies to investigate the applicability and reliability of dispersion models of different physical complexity in ACAs. Therefore a benchmark study had been initiated at the Institut für Neutronenphysik und Reaktortechnik (INR) of the Kernforschungszentrum Karlsruhe (KfK) to identify dispersion models which can be applied in ACA codes and to quantify the implications of different concepts of dispersion modelling (including the straight-line Gaussian) on the results of an ACA. The study comprises two parts. The first one deals with deterministic comparitive calculations to quantify the characteristic physical features of various dispersion models [10]. For this purpose a number of institutions had been asked for participitation with their atmospheric dispersion models (Table 1).

Participant	Institution	Type of model	Name of model
Dunst	Hamburg Univ., F.R.G.	Huang plume model	-
Dunst	Hamburg Univ., F.R.G.	Eulerian grid model	-
Gassmann	EIR, Switzerland	semi-Gaussian strata model	FOG
Jones	NRPB, U.K.	straight-line Gaussian plume model	ADMARC
Mikkelsen	RISO Nat. Lab., Denmark	Gaussian trajectory-puff model	RIMPUFF
Möllmann	KFA-Jülich, F.R.G.	Gaussian segmented plume model (trajectory)	MUSEMET
Päsler-Sauer	KfK, Karlsruhe,F.R.G.	straight-line Gaussian plume model	DOSI
Schnatz	Battelle Institut, Frankfurt/M., F.R.G.	Eulerian grid model	TRANSLOC
Schorling	IABG, Ottobrunn, F.R.G.	Lagrangian random walk model	-
Ulrich	Munich University, F.R.G.	Eulerian grid model	-

Table 1. Deterministic comparative study: Institutions and models participating in the study (from [10])

Different dispersion situations had to be calculated by the models, including stationary meteorological conditions as well as vertical shear of wind direction, and inversion situ-

ations. Additionally, the models were validated on the basis of four atmospheric dispersion experiments carried out at four different locations by four different laboratories. From this study the following conclusions could be drawn:

- most of the atmospheric dispersion situations examined are described quite satisfactory by the Gaussian-like trajectory- and puff models;
- the calculation of concentration distributions using the Gaussian-type models is reasonable, at least up to source distances of about 20 km to 50 km over uniform terrain; topographical effects have not been investigated;
- the more complex numerical and statistical models do not show apparent advantages except for more complicated meteorological conditions like wind shear and inversion;
- the required computer time is much lower (more than a factor of ten) for the Gaussian-type models.

The second part of the benchmark study has been designed to quantify the implications of using improved atmospheric dispersion models in ACA codes compared to the straight-line Gaussian model. For this purpose the influence of different concepts of dispersion modelling on the results of the ACA code UFOMOD [2] for assessing the consequences of nuclear accidents has been investigated. Because it is a general characteristic of an ACA code to estimate these consequences probabilistically, the second part of the benchmark study was referred to as probabilistic comparitive calculations. Due to the results of the deterministic part the Gaussian-like trajectory plume- and trajectory puff models MUSEMET [11] and RIMPUFF [12] have been chosen to participate in the probabilistic study.[1] Both models can also be used as straight-line models. To investigate also the influence of a non-Gaussian numerical model, additionally the Eulerian grid model TRANSLOC [13] took part, although this model type does not fulfill the requirement of reasonable computer time. For the sake of completeness it should be mentioned that a further trajectory model called RAPT [14] also performed the dispersion and deposition calculations necessary for the probabilistic comparison. This model had been developed to simulate atmospheric dispersion and deposition processes over a long distance range. But the horizontal grid size (25 km * 25 km) of this model was too coarse to process the calculated concentration distributions in UFOMOD. Therefore, RAPT had not been considered furthermore in the comparison.

The following chapter briefly describes the fundamentals and principle differences of the dispersion models which participate in the probabilistic study and it gives a short introduction into the UFOMOD code. Chapter 3 describes the meteorological input data and the different benchmark tasks. Finally, the results of the comparisons are presented and discussed.

The UFOMOD version B03 [26] used in this study refer to the old units Ci and rem for activity and doses, respectively. Therefore, these units are used throughout this report.

---

1 Work done at RISO Nat. Lab. had been supported by the Commission of European Communities, DG XI, under contract no. 85E1009

2. MODEL FUNDAMENTALS

2.1 The Diffusion-Advection-Equation

The basic differential equation for atmospheric dispersion problems is the Diffusion-Advection-Equation, which results from the gradient-transfer approach to turbulent diffusion [4], [15]

$$\frac{\partial C}{\partial t} = -\vec{v} \cdot \nabla C + \frac{\partial}{\partial x}\left(K_x \frac{\partial C}{\partial x}\right) + \frac{\partial}{\partial y}\left(K_y \frac{\partial C}{\partial y}\right) + \frac{\partial}{\partial z}\left(K_z \frac{\partial C}{\partial z}\right) \qquad (2.1)$$

with:

$C = C(\vec{r}, t)$	mean air concentration of radioactive material (Ci/m³)
$\vec{v} = \vec{v}(\vec{r}, t)$	mean three-dimensional vector of wind velocity (m/s)
K_x , K_y, K_z	x,y and z components of the eddy diffusivity (m²/s)

It is assumed that after the release into the atmosphere there exists no further source nor sink of the dispersing material. Eq. (2.1) expresses the conservation of the suspended material in an incompressible fluid. The left hand side represents the local temporal change of mean concentration at a location $\vec{r}$ at time t, which is accomplished by advection (first term on the right hand side) and by turbulent diffusion resulting from the turbulent fluctuations of the flow (second to fourth terms on the right hand side). The gradient transfer approach bases on the assumption that the turbulent flux F_i of the material is proportional to the mean concentration gradient, i. e.

$$F_i = -K_i \frac{\partial C}{\partial x_i}, \quad i = x, y, z \quad (\text{Ci m}^{-2}\,\text{s}^{-1}) \ .$$

F_i is the rate of turbulent transfer of the pollutant per unit area across a fixed surface down the mean concentration gradient.

2.2 The straight-line Gaussian plume model

It has been shown extensively in the literature (e.g. [17]) that the Gaussian distribution is an analytical solution of Eq. (2.1) if this equation is simplified by some basic assumptions:

1. the turbulent diffusion is of Fickian type, but anisotropic, i.e.

$$K_i = \text{const.}, \quad i = x,y,z$$
$$K_x \neq K_y \neq K_z \ ;$$

2. the mean wind field is considered as constant and it is directed along the x-axis, i.e.

$$\vec{v} = (u,0,0) = \textbf{const.} \ ;$$

3. the turbulent diffusion along the x-axis can be neglected compared to the advection by the mean wind u, i.e. $K_x = 0$;

4. stationary conditions ($\frac{\partial C}{\partial t} = 0$) .

With these assumptions Eq. (2.1) can be written as

$$u \frac{\partial C}{\partial x} = K_y \frac{\partial^2 C}{\partial y^2} + K_z \frac{\partial^2 C}{\partial z^2} \tag{2.2}$$

The most common model which satifies Eq. (2.2) together with appropriate boundary conditions is obtained from the assumption of a bi-Gaussian distribution of concentrations:

$$C(x,y,z) = \frac{\dot{Q}}{2\pi\sigma_y\sigma_z u} \exp\left(-\frac{y^2}{2\sigma_y^2} \right) \left\{ \exp\left(-\frac{(z-H)^2}{2\sigma_z^2} \right) + \exp\left(-\frac{(z+H)^2}{2\sigma_z^2} \right) \right\} \tag{2.3}$$

where

$$\sigma_j^2 = 2K_j t \,, \quad j = y,z \tag{2.4}$$

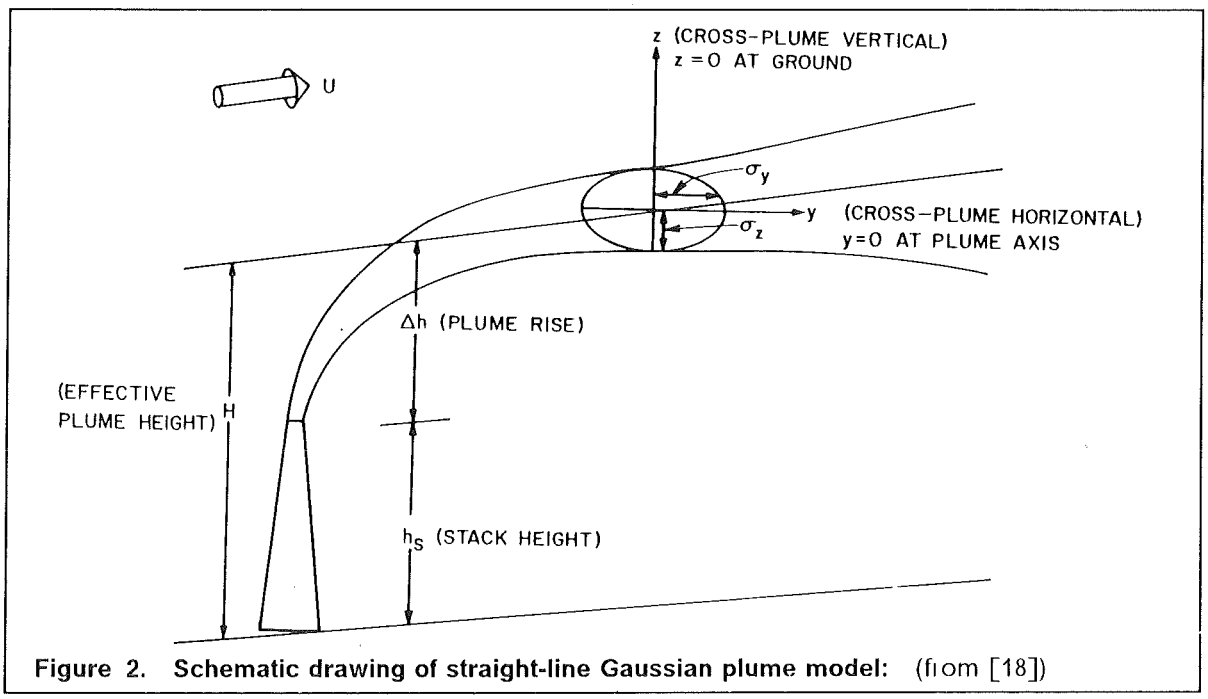

Figure 2. Schematic drawing of straight-line Gaussian plume model: (from [18])

Eq. (2.3) describes the distribution of concentration C at a point (x,y,z) on the leeside of a point source. It results from a continuous emission $\dot{Q}$ (in Ci/s) at an effective height H (in m) above ground in an uniform transport wind u (in m/s). X, y, and z are the rectangular coordintes of a cartesian frame of reference with its origin ($x = y = z = 0$) on the ground below the source; the x-axis is in the mean downwind direction, coinciding with the direction of the plume axis; y is the horizontal crosswind (lateral) distance from the

plume axis and z is the height above ground. Figure 2 is a schematic drawing which attempts to explain these definitions. The last exponential term on the right hand side of Eq. (2.3) accounts for reflection of the plume at the ground surface by assuming an image source of equal strength at $z = -H$ beneath the surface.

Height (m)	Stability Category	Diffusion Coefficients			
		p_y	q_y	p_z	q_z
50	A	1.503	0.833	0.151	1.219
	B	0.876	0.823	0.127	1.108
	C	0.659	0.807	0.165	0.996
	D	0.640	0.784	0.215	0.885
	E	0.801	0.754	0.264	0.774
	F	1.294	0.718	0.241	0.662
100	A	0.179	1.296	0.051	1.317
	B	0.324	1.025	0.070	1.151
	C	0.466	0.866	0.137	0.985
	D	0.504	0.818	0.265	0.818
	E	0.411	0.882	0.487	0.652
	F	0.253	1.057	0.717	0.486
180	A	0.671	0.903	0.025	1.500
	B	0.415	0.903	0.033	1.320
	C	0.232	0.903	0.104	0.997
	D	0.208	0.903	0.307	0.734
	E	0.245	0.903	0.546	0.557
	F	0.671	0.903	0.484	0.500

Table 2. Diffusion coefficients: Karlsruhe-Jülich-system as function of stability category and height (from: [19])

The diffusion parameters σ_y and σ_z (in m) are the lateral and vertical standard deviations of the assumed Gaussian distribution of concentration. They describe the lateral and vertical growth of the plume due to turbulent diffusion. Commonly it is assumed that they are power functions of travel distance (see Eq. (2.4) with $t = \frac{x}{u}$, $u = \text{const.}$):

$$\sigma_y = p_y x^{q_y} \tag{2.5}$$

$$\sigma_z = p_z x^{q_z} \tag{2.6}$$

The diffusion coefficients p_y, q_y, p_z, and q_z describe the turbulent structure of the atmosphere. Generally, they are determined by tracer experiments for different meteorological conditions. Table 2 shows a set of diffusion coefficients for different stability classes and different release heights. They have been derived from numerous tracer experiments

performed over rough terrain at nuclear research centers of Karlsruhe and Jülich [20], [21], [22], [23], [24]. The categorization of atmospheric stability is according to the Pasquill-Gifford typing scheme of turbulence (Table 3, [25]).

Pasquill-Gifford Notation	Stability Description
A	very unstable
B	moderately unstable
C	slightly unstable
D	neutral
E	moderately stable
F	very stable

Table 3. Pasquill-Gifford stability categories

The transport wind at the effective release height H is calculated from the power-law profile,

$$u = u_0 \left(\frac{H}{z_{ref}} \right)^p \quad , \tag{2.7}$$

where u_0 is the measured velocity at the reference height z_{ref} , generally, 10 m above ground. The exponent p depends on diffusion category. Values used in this study are given in Table 4 [1].

Diffusion Category	p
A	0.07
B	0.13
C	0.21
D	0.34
E	0.44
F	0.44

Table 4. Windprofile exponent

The quantity needed in ACAs to calculate doses is the time-integrated concentration at a given point in space. For radioactive releases the time-integrated concentration in air (T.I.C.) is expressed in Ci s m^{-3}. For a short-term, quasi-continuous release as in the case of accidents, the T.I.C. can be obtained from Eq. (2.3) simply by replacing the rate $\dot{Q}$ by Q_0, the total quantity released (in Ci).

$$C(x,y,z) = \frac{Q_0}{2\pi\sigma_y\sigma_z u} \exp\left(-\frac{y^2}{2\sigma_y^2}\right)\left\{\exp\left(-\frac{(z-H)^2}{2\sigma_z^2}\right) + \exp\left(-\frac{(z+H)^2}{2\sigma_z^2}\right)\right\} \quad (2.8)$$

The Gaussian plume model is strictly applicable for only a limited range of atmospheric and environmental conditions, because for its derivation it is assumed that the terrain over which the material is dispersing is uniform and that atmospheric conditions are constant. The restricting assumptions of stationary and homogeneous turbulent diffusion are partly compensated by using diffusion parameters which are determined experimentally. The classical Gaussian plume model has also been modified to consider slowly varying wind speed and diffusion categories [1]. Therefore, the meteorological data necessary to apply the model are single station measurements of wind speed, diffusion category and precipitation intensity, whenever the Gaussian model is modified to account for deposition processes (see Sect. 2.6). But changes of wind direction are not taken into account. Figure 3 shows the implications which pronounced changes of wind direction might have on the distribution of the T.I.C. near the ground. The meteorological conditions considered are taken as an example from a real meteorological recording. Applying the straight-line Gaussian model airborne pollutants are transported continuously into the inital north-easterly direction. Considering the changes of wind direction in the second and subsequent hours leads to a completely different concentration field contaminating the north-easterly neighbourhood and the areas west and south-west of the source. Therefore, extensions of the conventional Gaussian model for computation of the dispersion of suspended material have been developed with regard to changing weather conditions, especially, wind direction.

2.3 *The volume source model MUSEMET*

This model is based on the assumption that the weather conditions (wind direction, wind speed and diffusion category) are known and may be assumed constant in consecutive time intervals (e.g. hourly intervals). The basic idea is to regard the volume elements of the concentration distribution at the end of time interval k as point sources for diffusion calculation in the next time interval (k + 1) with new weather conditions. Figure 4 schematically describes the idea of the volume source model. The concentration distribution C_k at the end of each time interval Δt_k with constant weather conditions is composite of the concentrations from all the infinitesimal volume elements $dx_k dy_k dz_k$ that can be taken as point sources of inifinitesimal source strength dq_k for the diffusion calculation in the next time interval Δt_{k+1} with new weather conditions. The integral contribution of all these point sources results in a Gaussian distribution of concentration C_{k+1}.

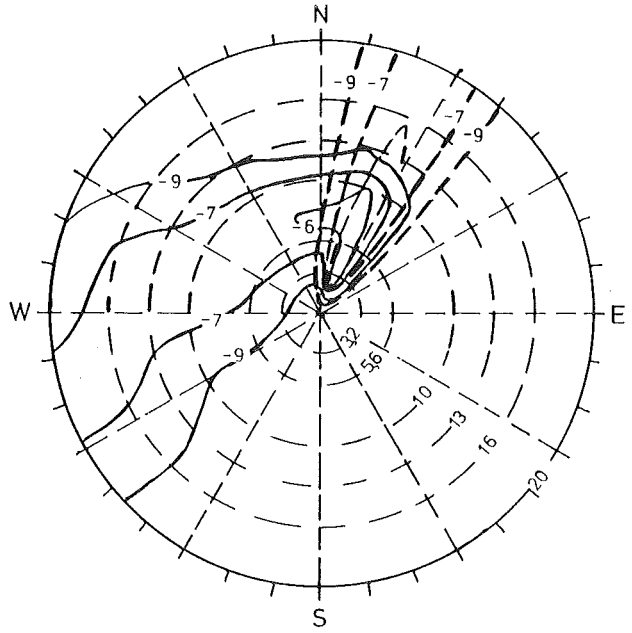

Figure 3. Difference between straigth-line and trajectory modelling:

broken lines: straight-line Gaussian model
full lines: Gaussain trajectory model
the isolines depict the decadic logarithms of normalized concentration distribution; radial distances are in km

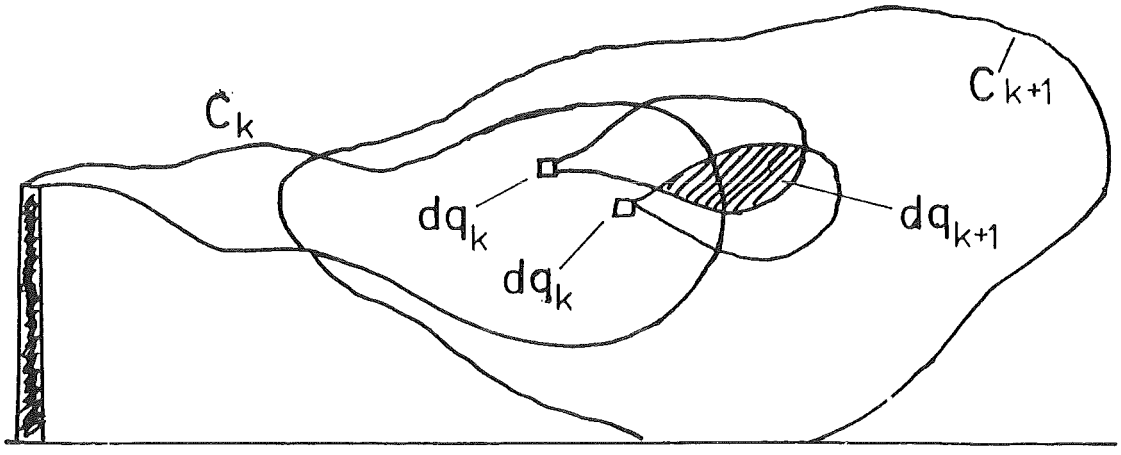

Figure 4. Schematical drawing of the volume source model: (from [27])

It has been shown in [11] that the T.I.C. in the n-th time interval can be written similar to Eq. (2.8) as

$$C_n(x,y,z) = \frac{Q_0}{2\pi\sigma_{y,eff}\sigma_{z,eff}u_n} \exp\left(-\frac{\eta_n^2}{2\sigma_{y,eff}^2}\right) \left\{\exp\left(-\frac{(z-H)^2}{2\sigma_{z,eff}^2}\right) + \exp\left(-\frac{(z+H)^2}{2\sigma_{z,eff}^2}\right)\right\}\Delta f_n \quad (2.9)$$

with:

C_n	T.I.C. at the point x,y,z, in the n-th time interval (Ci s m^{-3})
Q_0	total quantity released (Ci)
H	effective release height (m)
u_n	constant wind speed (m/s) at height H during the n-th time interval calculated according to Eq. (2.7)
x,y,z	downwind, crosswind, and vertical coordinates of a mathematical cartesian system with its origin below the source on the ground (see Figure 5)

For taking into account the changes of wind direction, the originally straight-line axis of the plume is turned into the direction of the real trajectory at the beginning of each time intervall Δt_n . This transformation is performed by successive translations and rotations relative to the fixed cartesian coordinate system. (Figure 5).

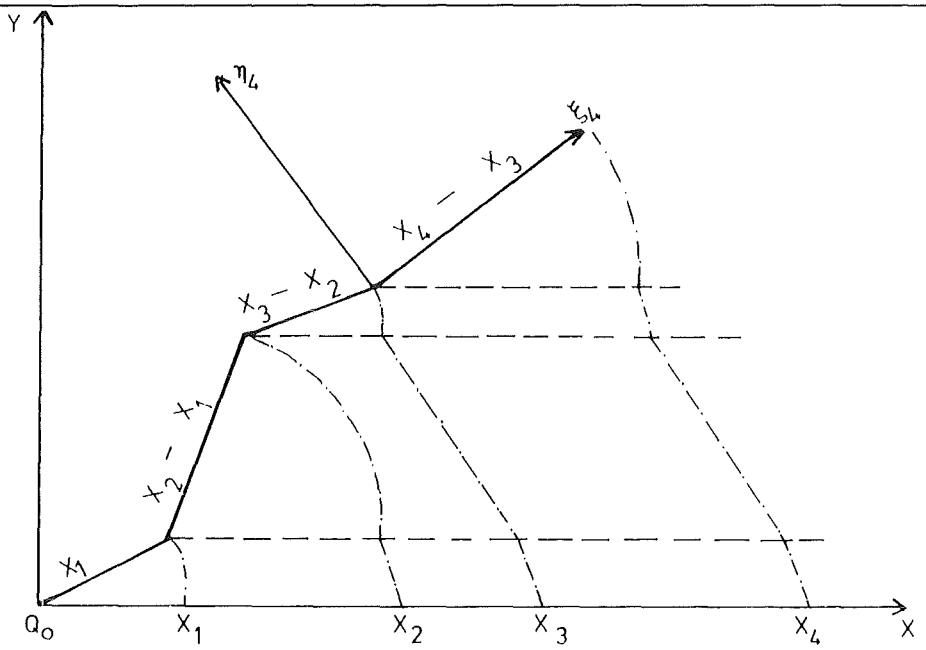

Figure 5. Determination of trajectories in MUSEMET

Thus

$$\eta_n = \frac{1}{u_n}\left\{u_{x,n}\left[y - \sum_{k=1}^{n-1} u_{y,k}(t_k - t_{k-1})\right] - u_{y,n}\left[x - \sum_{k=1}^{n-1} u_{x,k}(t_k - t_{k-1})\right]\right\}$$

with:

$u_{i,k}$ wind components in the k-th time interval relative to the fixed system, $i = x,y$

is the crosswind distance from the trajectory in the n-th time interval.

The effective dispersion paramteres $\sigma_{i,eff}$, $i = y,z$, are obtained as the sum over the variances $\sigma_{i,k}^2$ in the individual time intervals

$$\sigma_{i,eff}^2 = \sigma_{i,eff}^2(t) = \sum_{k=1}^{n-1} \sigma_{i,k}^2 + \sigma_{i,n}^2(t - t_{n-1}), \quad i = y,z$$

where, if Fickian diffusion is assumed, the dispersion parameter $\sigma_{i,k}$ in the k-th time interval $\Delta t_k = t_k - t_{k-1}$ can be written as

$$\sigma_{i,k}^2 = \sigma_{i,k}^2(t_k - t_{k-1}) = \sigma_{i,k}^2(t_k) - \sigma_{i,k}^2(t_{k-1})$$

or, if power law functions are assumed

$$\sigma_{i,k}^2 = p_{i,k}^2 (x_k^{2q_{i,k}} - x_{k-1}^{2q_{i,k}})$$

$$= p_{i,k}^2 \left\{\left[\sum_{m=1}^{k} u_m(t_m - t_{m-1})\right]^{2q_{i,k}} - \left[\sum_{m=1}^{k-1} u_m(t_m - t_{m-1})\right]^{2q_{i,k}}\right\}, \quad i = y,z$$

Wind direction,wind speed and diffusion category in consecutive time intervals are obtained from synoptic measurements at a single meteorological station which can be considered representative for the source location and the surrounding region. This, of course, limits the validity of the model to situations where the wind field and turbulence can be assumed to be horizontally homogeneous throughout the whole dispersion area.

The factor Δf_n in Eq. (2.9) represents a correction with respect to the calculation of the T.I.C.. Instead of carrying out the integration from $-\infty$ to $+\infty$ passing the point of reference, as it is common practice when using the straight-line Gaussian model, integration now is performed only for the duration of the respective time interval, resulting in a difference of error functions [28].

$$\Delta f_n = \frac{1}{2}\left\{\mathrm{erf}\left(\frac{u_n(t_n - t_{n-1}) - \xi_n}{\sqrt{2}\,\sigma_{y,eff}}\right) - \mathrm{erf}\left(\frac{-\xi_n}{\sqrt{2}\,\sigma_{y,eff}}\right)\right\}$$

$$\mathrm{erf}(x) = \frac{2}{\sqrt{\pi}}\int_0^x \exp(-s^2)ds \quad \text{error function}$$

with

ξ_n downwind coordinate of the point of reference related to the trajectory in the n-th time interval.

$$\xi_n = \frac{1}{u_n}\left\{u_{x,n}\left[x - \sum_{k=1}^{n-1} u_{x,k}(t_k - t_{k-1})\right] - u_{y,n}\left[y - \sum_{k=1}^{n-1} u_{y,k}(t_k - t_{k-1})\right]\right\}$$

Thus, Δf_n describes that part of the plume which passes by the point of reference during the n-th time interval.

With the volume source model a Gaussian-type model has been developed which, in contrast to the conventional straight-line plume model, takes into account temporal changes of meteorological conditions. The T.I.C. are calculated across straight-line segments of a trajectory. The orientation of each segment and thus of the whole trajectory is determined by the wind directions and wind speeds in consecutive time intervals.

2.4 *The puff diffusion model RIMPUFF*

The puff model RIMPUFF has been developed to describe the dispersion of time-dependent atmospheric releases taking into account non-stationary and non-homogeneous atmospheric conditions [12]. A puff is defined as a short-time release of a few seconds up to a few minutes. Thus, a continuous release can be simulated by a series of individual puffs each containing the same release rate. Figure 6a depicts a typical instantaneous plume together with the instantaneous concentration and the long-term average plume concentration. The puff model prediction is shown in Figure 6b.

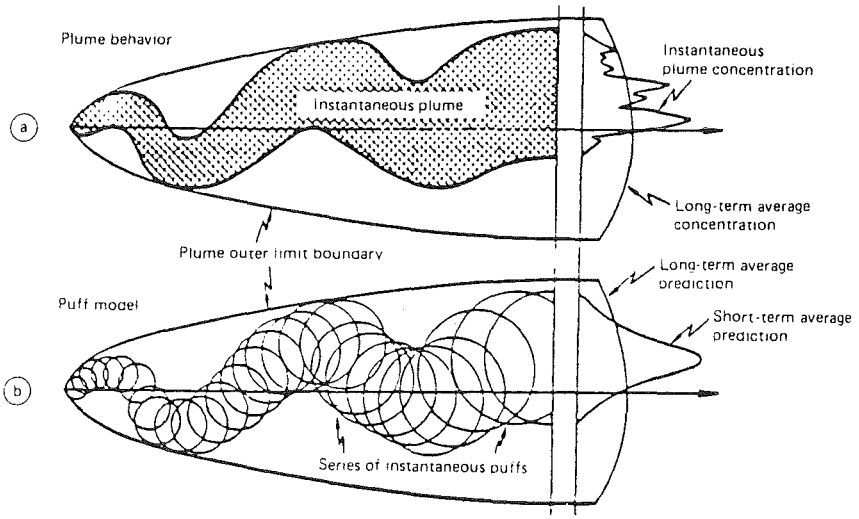

Figure 6. Schematic drawing of diffusion of a plume: simulation by a finite number of puffs,in case of changing wind direction (from [12])

The puffs are advected downwind by a wind field which is updated after certain time intervals ,e.g. hourly intervals. It is assumed that the short-term average concentration is Gaussian-shaped and that it represents a reasonable approximation to ensemble-averaged instantaneous plume concentration profile. The long-term average concentration of the puff model is expected to be identical to the long-term concentration of Figure 6a.

Each puff contributes to the spatial concentration distribution which corresponds to the three-dimensional Gaussian solution of Eq. (2.1) for an instantaneous point emission [17]:

$$C_i(x,y,z) = \frac{Q_i}{(2\pi)^{3/2}\sigma_x\sigma_y\sigma_z} \exp\left(-\frac{1}{2}\left[\frac{(x-ut)^2}{\sigma_x^2} + \frac{(y-vt)^2}{\sigma_y^2} \right] \right) \left\{ \exp\left(-\frac{(z-H)^2}{2\sigma_z^2} \right) + \exp\left(-\frac{(z+H)^2}{2\sigma_z^2} \right) \right\} \quad (2.10)$$

with:

C_i	contribution of puff i to concentration at point x,y,z at time t (Ci/m³);
Q_i	total amount of released quantity carried by the i-th puff (Ci);
σ_x	longitudinal diffusion parameter (m); generally, $\sigma_x = \sigma_y$ is assumed;
x,y,z	rectangular coordinates of a three-dimensional grid containing the whole area over which material is dispersing;
u,v	time- and space dependent components of wind vector in the x and y direction, respectively (m/s).

Then the total concentration at each point is calculated by summing the contributions from all puffs in the grid at each time step. Once a puff is released, it is advected over a rectangular advection grid by the mean wind vector at its center-of-mass position at each time step [12]. The inhomogeneous wind field is estimated from a network of available observations by the method of objective wind analysis. A $1/r^2$-weighting function, where r is the distance from the grid point to the measurement station, is used for the interpolation [29]. Of course, the wind field can be determined by measurements at a single point at or nearby the source location as it is done in the plume model MUSEMET, restricting the validity of the model to homogeneous meteorological situations. At each grid point the vertical wind profile is calculated according to Eq. (5). Depending on the density of the meteorological observation network and the quality of the horizontal wind field the RIMPUFF version used in the comparative calculations is implicitly able to take account of topographical effects in the atmospheric flow field. Recently, RIMPUFF has been extended by a horizontal puff-splitting scheme to model explicitly the dispersion of pollutants emitted in complex terrain [30]. RIMPUFF is also able to consider vertical wind shear [12]. But this option has not been used in the comparative study.

As the individual puffs advect with the wind, they grow in size in accordance with the local diffusion category. Fundamentally, the expansion of a single puff is related to the relative diffusion process which is most conveniently described as function of local turbulence intensities and downwind distances [31], [32]. Alternatively, in the absence of turbulent intensity data, the expansion of the puff can be described by suitable plume diffusion parameters, e.g. the Karlsruhe-Jülich-system (see Table 2, Eq. (2.5 - 2.6)). The

sigma values after a given advection step Δx and for a given local stability are obtained by differentiation of Eq. (2.5 - 2.6) and, subsequently, integration:

$$\sigma_j(x + \Delta x) = \left(\sigma(x)^{1/q_j} + p_j^{1/q_j} \cdot \Delta x\right)^{q_j}, \quad j = x,y,z\,. \tag{2.11}$$

To account for non-homogeneous and non-stationary dispersion scenarios it is neccessary that the meteorological data (wind direction, wind speed, diffusion category and precipitation intensity) are available from several representative stations in the area where the material is dispersing. This is the first major difference between RIMPUFF and MUSEMET, which assumes that these data of one single representative station are known.

The second basic difference between both models is illustrated in Figure 7.

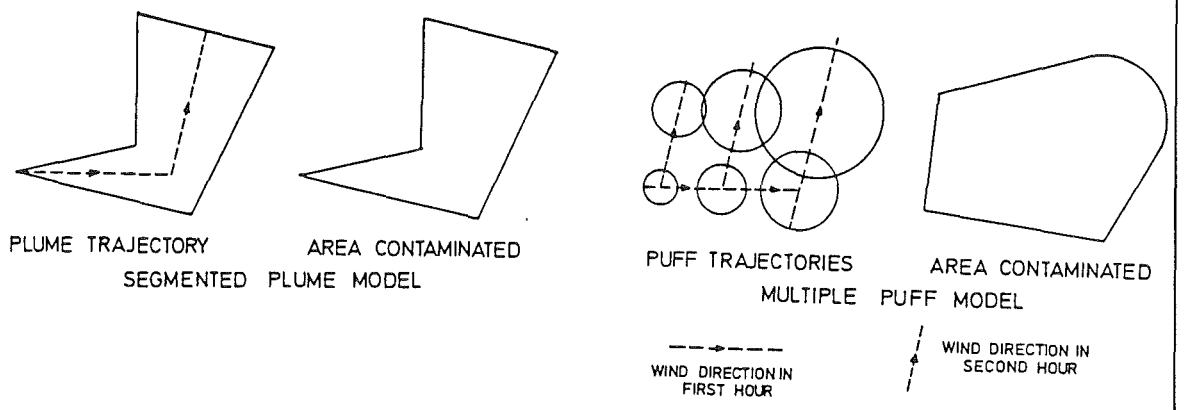

Figure 7. Illustration of plume and puff models: (from [33])

The segmented plume model MUSEMET advects the suspended material along one single trajectory which is divided into several straight-line segments. The direction and the length of each segment are determined by the prevailing meteorological conditions assumed as constant in consecutive hourly time intervals. In the multiple puff model RIMPUFF all puffs released experience a change of meteorological conditions instantaneously. Each individual puff will follow its own trajectory according to the local meteorological conditions in an inhomogeneous meteorological field.

2.5 *The Eulerian grid point model TRANSLOC*

The dispersion models described so far are based on the analytical Gaussian solution of the Diffusion-Advection-Equation. A different approach is to transform the differential

equation into a set of finite differences and to solve these difference equations numerically on a three-dimensional Eulerian grid using appropriate difference schemes.

The model TRANSLOC [13] uses the method of fractional steps [34] to carry out the time integration. For the solution of the advective part the Carlson-scheme is applied [35]. Problems with mass conservation [36] are controlled and minimized by a continuous calculation of mass balance. Numerical pseudo-diffusion which can arise in the solution of the advection part is avoided by approximation of the vertical wind profile as a step-function. The diffusion part is solved by the application of the Crank-Nicholson method [35]. To avoid numerical instabilities the time steps are chosen appropriately depending on the grid size and the values of the vertical diffusion coefficient in each vertical layer. On the other hand, all numerical schemes used in TRANSLOC can be used in the fully implicit mode which always provides computational stable solutions [37].

The vertical eddy diffusion coefficient is based on Wu [38].

$$K_z(z) = \sqrt{\left(\frac{\partial u}{\partial z}\right)^2 - a\,\frac{g}{\Theta}\,\frac{\partial \Theta}{\partial z}}\left(\frac{\kappa z}{1+\frac{\kappa z}{\lambda}}\right)^2 \qquad (2.12)$$

with

u	mean horizontal wind speed (m/s) in vertical level z;
Θ	mean potential temperature (°K);
g	acceleration of gravity (m/s²);
a	ratio of K_h to K_m;
K_h	eddy exchange coefficient of heat (m²/s);
K_m	eddy exchange coefficient of momentum (m²/s);
κ	v. Karman's constant;
λ	turbulent mixing length (m), depending on stability.

For stable atmospheric conditions and assuming $a = 1.13 = \text{const.}$, imaginary values of K_z are possible, meaning that turbulence is completely suppressed. Therefore, Wu's formulation of K_z has been modified for TRANSLOC [39]. According to an idea of Ellison (see for example [40]) a is calculated as a decreasing function of the Richardson number, Ri, which increases with increasing stability. The Richardson number is defined as

$$Ri = \frac{\frac{g}{\Theta}\frac{\partial \Theta}{\partial z}}{\left(\frac{\partial u}{\partial z}\right)^2}$$

Then the Richardson flux-number, $Rf = a\,Ri$, can take values which are less than one, even if $Ri > 1$, indicating that a turbulent vertical transfer is still existing mainly due to the mechanically induced turbulence.

The horizontal diffusion coefficients are set to $K_x = K_y = 2\,K_z^{max}$ where K_z^{max} is the absolute maximum of K_z in the mixing layer.

To calculate K_z and to predict the advection it is necessary to know wind- and temperature profiles at each grid point. Generally, only surface observations of wind direction and wind speed can be obtained routinely on an hourly basis and the vertical profiles of wind speed have to be estimated by using, for example, Eq. (2.7) without considering vertical changes of wind direction. Since the exponent in Eq. (2.7) depends on stability, information about the diffusion categories is also needed. Measurements of the vertical temperature profiles are carried out routinely only two or four times a day on a rather coarse network of specific radiosonde stations. Therefore, some reasonable temporal and spatial approximations have to be found for the vertical temperature profiles, using measurements from a few stations in or nearby the region where the pollutants are dispersing.

The principle difference between the Gaussian-type models and the numerical model is the capability of the numerical model of considering explicitly the three-dimensional inhomogeneous and instationary structure of the wind- and turbulence field. But this advantage might be lost if the necessary meteorological input data are not available with an appropriate quantity and quality.

2.6 *Modelling of deposition processes*

During the dispersion material may be removed from the plume by dry and wet deposition resulting in contamination of the ground.

Dry deposition is due to the contact of the plume on surfaces, such as walls, leaves and ground; gravitational settling will not yet be considered. It is assumed that the resulting surface contamination C_d (in Ci/m^2) is proportional to the T.I.C. C near the ground, generally, in 1m height [4]:

$$C_d = v_d C \tag{2.13}$$

where v_d is referred to as the dry deposition velocity. It depends on the physical and chemical form of the isotopes released: noble gases which will not be deposited, particulate material (aerosols), elemental and organically bound iodine. Since it is assumed for the hypothetical source terms used in this study (see Chapter 3) that iodine will be released to 100% as particulates, only aerosol deposition is relevant. In this study a value $v_d = 0.001$ m/s is used for the corresponding dry deposition velocity.

Generally, in Gaussian-type dispersion models the loss due to dry deposition is accounted for by reducing appropriately the source strength. This so called source depeletion model [4] implicitly assumes that the depletion occurs over the whole depth of the plume rather than at the surface; therefore, the shape of the plume's vertical profile does not change.

But this assumption does not correspond to the physical reality because the deposition only causes a reduction of material in the lowest layer near the ground. Therefore, in the numerical model TRANSLOC the effect of dry deposition is taken into account by reducing the concentration only in the lowest vertical layer. Thus a vertical gradient of concentration builds up leading to a downward flux of radionuclides proportional to the vertical gradient.

The mechanism contributing to wet deposition on the ground is washout. It describes the contamination of the ground by rain, snow and hail formed above and falling through the plume and thereby collecting particulates and soluble gases or vapours; rainout, which refers to the removal of airborne constituents during the formation and growth of rain drops in the plume, will not be considered. The resulting source depletion is accounted for in all participating dispersion models by applying the following correction factor [4]:

$$f_p(x) = \exp\left(-\frac{\lambda}{u}x\right) \tag{2.14}$$

where λ is the washout coefficient (s^{-1}), u the wind speed (m/s) in release height H, and x the downwind distance (m). The coefficient λ describes the amount of precipitation scavenging and the rate of wet deposition on the ground. It depends on the physico-chemical porperties of the airborne material and the precipitation intensity. Generally, λ is determined from a power-law function of precipitation intensity with appropriate coefficients [41]. In the present study precalculated values of λ are used which have been evaluated for gaseous and particulate radionuclides for three different precipitation classes [42]. Additionally, a characteristic duration of rainfall is linked to each intensity class, which is derived from a ten years record of rain intensity at the nuclear research centre Karlsruhe. The values of the washout coefficent and precipitation duration for aerosol deposition used in this study are shown in Table 5 for different rainfall intensities.

precipitation intensity (mm/h)	washout coeffient (s^{-1})	duration of rainfall (s)
< 1	3.40E-5	1800
1 - 3	1.17E-4	2628
> 3	3.33E-4	2088

Table 5. Wet deposition parameters for aerosols: (from: [42])

Since it is assumed that the rain is falling through the whole vertical extent of the plume the contribution of wet deposition to ground contamination $C_w(x, y)$ (Ci/m^2) is calculated by multiplying λ with the vertically integrated T.I.C..

$$C_w(x, y) = \lambda \int_0^z C(x,y,z)dz \tag{2.15}$$

where λ is assumed to be constant over the entire vertical extension of the plume.

The total ground contamination is simply given as the sum of the dry and wet deposition contributions.

2.7 *Plume rise and height of mixing layer*

Because it was not the task to compare different modelling of plume rise it has been decided that each model uses precalculated values of plume rise which only depend on wind speed and stability class.

Diffusion category	Wind speed u_0 (m/s)	Plume rise (m)
A	1	290
	2	140
	3	85
	4	64
B	1	260
	2	120
	3	78
	4	57
C	1	225
	2	103
	3	70
	4	50
D	1	165
	2	85
	3	60
	4	40
	5	30
	6	22
	8	13
E	1	120
	2	68
	3	47
	4	37
F	1	70
	2	45
	3	35
	4	28

Table 6. Approximated plume rise for an FK2 release

These values (Table 6) have been calculated by Päsler-Sauer [43] on the basis of the FK2-release of the German Risk Study - Phase A [1] using Brigg's formulae, because it was originally intended to base the ACAs in the present investigation on the FK2 source term.

The mixing layer is the part of the atmosphere above the ground where most of the atmospheric dispersion and deposition processes take place and where the radionu-

clides are well mixed due to thermal and mechanical turbulence. The upper boundary of this layer varies with stability. The Gaussian-type models MUSEMET and RIMPUFF do not explicitly model the daily variations of the height of the mixing layer. Preselected values depending on the stability class are used (Table 7). Generally, it is assumed that an inversion layer forms the upper boundary of the mixing layer which cannot be penetrated by the plume. Therefore, neither the final plume rise height nor the vertical diffusion can exceed the mixing height. Multiple perfect reflection of the plume at this lid is taken into account by limiting the vertical diffusion parameter σ_z according to [44].

$$\sigma_z = \sigma_z^{max} = 0.8H_{mix}, \quad \text{if } \sigma_z \geq \sigma_z^{max}$$

where H_{mix} denotes the height of the mixing layer (in m). Further, it is assumed that once a certain height of the mixing layer is reached during the course of the day, it cannot decrease, even if the atmospheric stratification turns to more stable conditions.

It is not necessary to define or to model the height of the mixing layer explicitly in the numerical model TRANSLOC because in the upper layers the stability dependent turbulent diffusion coefficient K_z will generally decrease and, thus, the vertical mixing will diminish.

Diffusion category	Height of mixing layer (m)	
	MUSEMET	RIMPUFF
A	1600	1600
B	1200	1200
C	800	800
D	560	600
E	320	300
F	200	200

Table 7. Height of mixing layer

2.8 *The accident consequence code UFOMOD*

UFOMOD is a computer code for probabilistic assessments of the consequences after accidents in nuclear facilities. Figure 8 sketches the basic features of the UFOMOD version B03 used in this study [26].

The starting point is the so-called source term which contains the amount and form of each radionuclide release to the atmosphere, the time when the release occurs, its time dependency, and energy content. Atmospheric dispersion and deposition lead to a spatial and temporal distribution of radioactive material in the air and on the ground. These can be converted to distributions of dose in man. The major exposure pathways are external irradiation from the plume and from deposited activity, and internal irradiation from radioactive material taken into the body by inhalation and by ingestion of contaminated food.

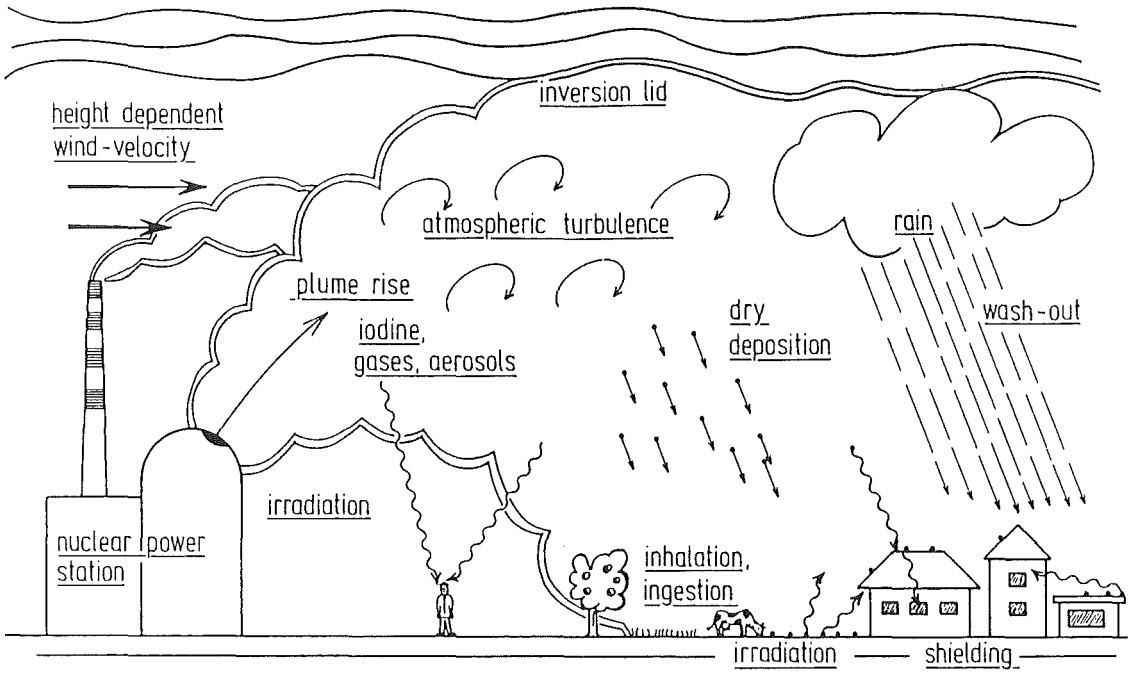

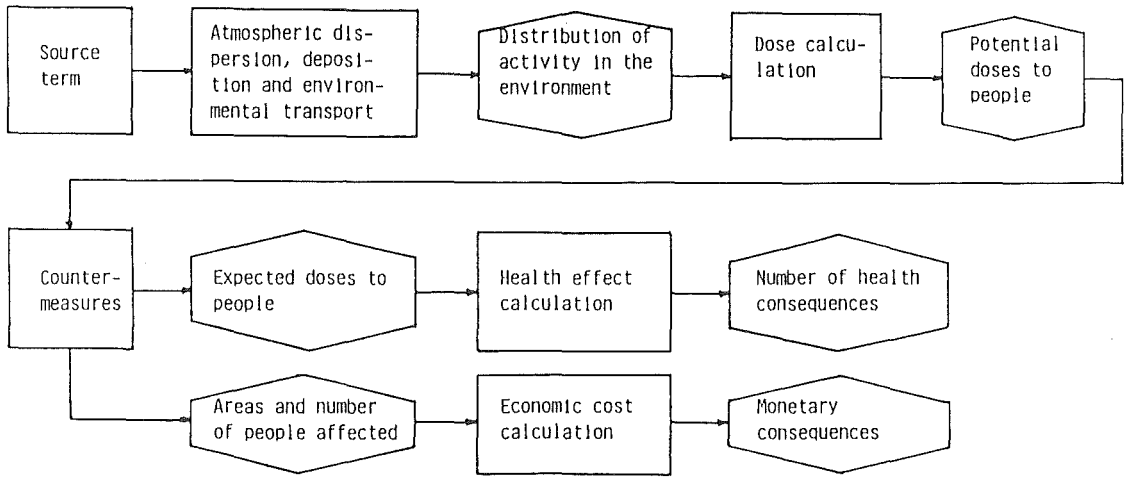

Figure 8. Basic features of the ACA program system UFOMOD: (from [33])

A realistic estimate of the exposure of the population must take into account protective actions. Their extent and duration depend on the scale of the accident.

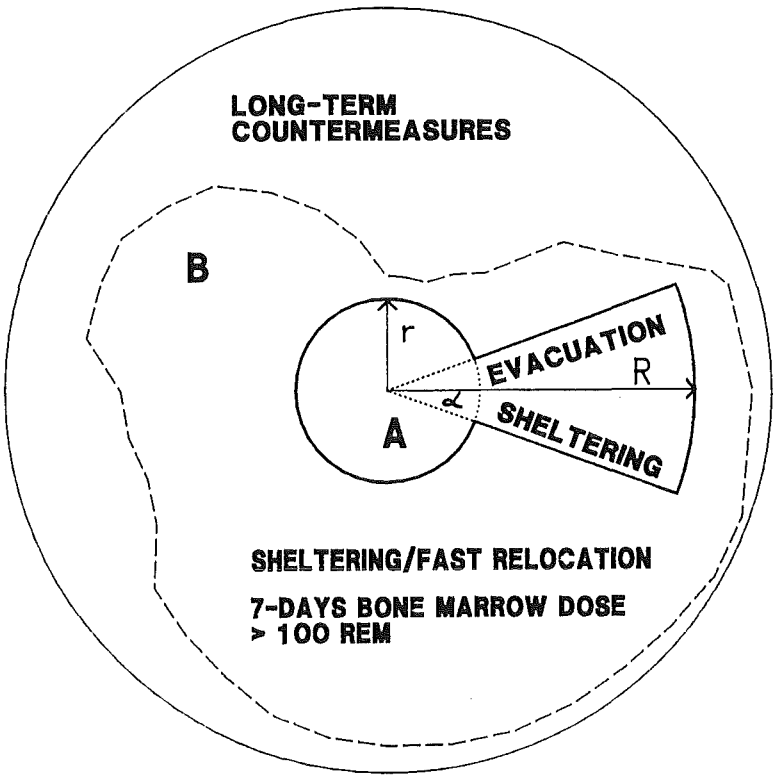

Figure 9. UFOMOD: modelling of protective actions

Figure 9 sketches the modelling of countermeasures in UFOMOD. In the early phase of an accidental release sheltering and evacuation are the major countermeasures affecting people. The evacuation area A is defined geometrically as a keyhole with an inner radius r, an outer radius R, and an sector angle $\alpha = 30°$. The sector is always directed into the transport direction prevailing at the beginning of the release. Thus, the size and the direction of the evacuation area A do not depend on the type of dispersion model.

In the intermediate phase and in the longer term people may be relocated for varying periods until the radiation levels have been reduced by radioactive decay and/or remedial measures such as decontamination. Countermeasures may also be applied to restrict the production and distribution of contaminated foods. These actions whose extent might be influenced by the kind of atmospheric dispersion models are summarized in Table 8.

Action	Main aim ⇒ mitigation of	Dose-dependent action
Fast Relocation	early fatalities due to groundshine	yes Area B (Figure 9)
Relocation	late effects due to groundshine	yes long-term action (Figure 9)
Decontamination	late effects due to groundshine	yes long-term action (Figure 9)
Interdiction of food distribution	late effects due to ingestion	yes long-term action (Figure 9)

Table 8. Dose-dependent countermeasures influenced by different atmospheric dispersion models: (adapted from [2])

The areas which are affected are defined by isolines of potential organ doses exceeding certain intervention levels. Adjacent to the area A an area B can appear where sheltering and fast relocation take place. Outside area B protective actions against long-term exposure might be taken. These are relocation, decontamination, and food-bans.

Finally, the incidence of health effects in the exposed population after taking due account of the application of protective actions and interdictions is evaluated. There are two broad effects that are considered. Early health effects only occur if relatively high treshold doses are exceeded and they may arise within days, weeks or months after exposure. They include death and varying forms of health impairment which may be temporary or more prolonged. The late health effects comprise fatal and non-fatal cancers in the exposed population and hereditary effects in their descendants. In contrast to early effects, they are primarily stochastic in nature. There is a delay, which may be many years, during which no individual experience the injury. After this latent period, the expression of the total number of health effects in the population may take place over a period of many years.

Thus, based on the temporal source term characteristics and the meteorological conditions time-integrated air concentration and ground contamination patterns are calculated by the atmospheric dispersion and deposition model. These spatial concentration fields are used as input to subsequent subroutines of UFOMOD to calculate distribution functions of air concentration, contaminated areas, organ doses and health effects together with areas and the number of persons affected by countermeasures.

3. METEOROLOGICAL DATA, SOURCE TERMS, BENCHMARK TASKS AND COMPUTATIONAL EFFORT

3.1 Meteorological data

For the study a large amount of hourly and 3-hourly recorded synoptic data and wind measurements have been provided by the German Weather Service for the year 1975. Most of the stations are located within a 200 km circle around the nuclear site of Biblis which was the reference nuclear installation of the German Risk Study - Phase A [1]. In addition, the German Weather Service provided data of vertical temperature profiles measured twice daily by radiosondes at the aerological stations Essen and Stuttgart. The 12 UTC[2] measurements have been considered representative for the day-time from 6 UTC to 18 UTC and the 00 UTC data for the night-time from 19 UTC to 5 UTC [45]. These temperature profiles are necessary to calculate the vertical turbulent diffusion coefficients K_z in the model TRANSLOC. All the data were sent to the participating institutions to prepare the meteorological recordings as input data convenient for their models [45], [46]. All models need at least hourly recordings of wind speed, wind direction, stability category and precipitation intensity. Wind speed and wind direction near the ground level (generally at 10 m height) are routine measurements at all meteorological stations. The classification of atmospheric stability is performed by appplying the Klug-Manier scheme [47], [48] using routine synoptic data. The Klug-Manier classes can be converted easily to the Pasquill-Gifford stability categories (see Table 3). The amount of rainfall in the locality of a synoptic station is generally available only in the form of the "present weather" code (WW-code). Then representative intensity values have to be assigned to the corresponding code numbers (50 to 99 indicating various types of precipitation at the time of observation, 20 to 29 describing precipitation in the previous hour, see for example [42]). For this study the German Weather Service provided hourly intensity values for some few stations but only for the period from May, 1 to September, 27. For the rest of the year no precipitation information was available.

As already mentioned in the Introduction, it is necessary in probabilistic ACAs to repeat the atmospheric dispersion calculations with a large amount of weather sequences representing different characteristic meteorological situations to predict the full distribution of consequences which may occur following a postulated accidental release. To get a representative sample of weather sequences all possible hourly weather situations of the whole year have been classified according to wind direction, wind speed, stability category, and precipitation intensity measured at Frankfurt/Airport [49]. The intension of such a categorization is to group all weather situations present in the meteorological data base which give rise to the similar near-to-the-site predictions of the accident consequences. By grouping the weather conditions, the probability of occurrence of each category may be determined directly. Weather sequences, identified by the time of their start relative to the beginning of the year, are then selected randomly from each category, thus ensuring that the full range of possible weather situations is covered. Because

---

2 UTC = **U**niversal **T**ime **C**oordinated

no weather data were available from the site of Biblis, the sampling has been carried out with the data of the closest meteorological station Frankfurt/Airport which was regarded as representative for the nuclear site itself and the region near to the site. Altogether 95 characteristic weather sequences have been selected. Their starting times relative to January,1, 00 UTC and their probabilities of occurrence are shown in Table 9 and Table 10, respectively.

NO. OF SEQUENCES	STARTING TIMES (H)									
1 – 10	197	239	324	335	344	458	765	773	782	981
11 – 20	998	1,005	1,237	1,299	1,398	1,498	1,566	1,793	1,802	1,807
21 – 30	2,257	2,297	2,460	2,551	2,576	2,617	2,638	2,805	2,972	3,041
31 – 40	3,057	3,118	3,216	3,285	3,582	3,610	3,738	3,836	4,028	4,051
41 – 50	4,060	4,061	4,063	4,067	4,149	4,151	4,185	4,234	4,239	4,300
51 – 60	4,432	4,433	4,445	4,584	4,792	4,825	4,935	5,051	5,277	5,496
61 – 70	5,497	5,499	5,510	5,518	5,621	5,668	5,675	5,676	5,832	5,892
71 – 80	5,931	6,052	6,061	6,267	6,320	6,356	6,577	6,580	6,774	6,886
81 – 90	6,888	6,889	6,982	7,045	7,113	7,114	7,581	7,593	7,596	7,889
91 – 95	7,890	7,936	8,017	8,140	8,166					

Table 9. Starting times of 95 weather sequences

NO. OF SEQUENCES	PROBABILITIES									
1 – 10	0.0033	0.0023	0.0019	0.0010	0.0540	0.0011	0.0014	0.0026	0.0110	0.1320
11 – 20	0.0005	0.0032	0.0078	0.0101	0.0003	0.0006	0.0009	0.0100	0.0037	0.0013
21 – 30	0.0030	0.0197	0.0125	0.0007	0.0212	0.0005	0.0002	0.0019	0.0005	0.0122
31 – 40	0.0001	0.0257	0.0001	0.0007	0.0016	0.0071	0.0262	0.0288	0.0012	0.0002
41 – 50	0.0001	0.0002	0.0002	0.0010	0.0002	0.0007	0.0002	0.0007	0.0016	0.0036
51 – 60	0.0007	0.0002	0.0001	0.0917	0.0024	0.0008	0.0106	0.0354	0.0158	0.0029
61 – 70	0.0001	0.0041	0.0148	0.0014	0.0176	0.0054	0.0003	0.0001	0.0006	0.0474
71 – 80	0.0116	0.0062	0.0137	0.0018	0.0005	0.0114	0.0094	0.0054	0.0116	0.0019
81 – 90	0.0082	0.0047	0.0168	0.1030	0.0008	0.0006	0.0002	0.0002	0.0061	0.0005
91 – 95	0.0016	0.0459	0.0008	0.0614	0.0013					

Table 10. Probabilities of occurrence of the 95 weather sequences

Due to the lack of precipitation data from January to April and from the end of September to December two different groups of weather sequences can be distinguished which allow

- dispersion calculations during the "winter" without consideration of wet deposition (47 sequences with starting times from 197 to 2805 and from 6577 to 8166)
- dispersion calculations during the "summer" considering also wet deposition (48 sequences with starting times from 2972 to 6356)

3.2 *Source terms*

In the initial phase of the study it was intended to consider a source term which, in the beginnig of the release, showed a similar temporal behaviour as the FK2 source term of the German Risk Study - Phase A [2], but with an additional fourth release phase starting 36 hours after the initial release (Figure 10).

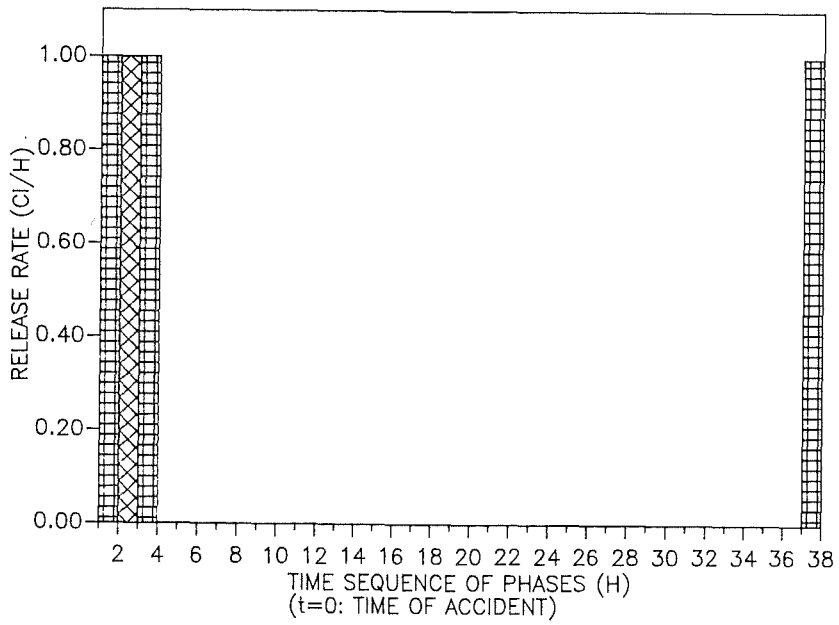

Figure 10. Temporal behaviour of modified FK2 source term: the duration of each phase is one hour

This combination of release phases allows to model an FK2 release as well as a reelase after a late overpressure failure of the containment. The large lag between the three consecutive phases in the beginning and the fourth phase ensures that the atmospheric conditions prevailing at the corresponding times can be considered as independent.

Later on, in the framework of the German Risk Study - Phase B, new source terms came into discussion [50] which avoid the single peak release due to the overpressure failure by a controlled venting of the containment through aerosol and iodine filters. Therefore, it was decided to construct a new artificial source term for the present study adapted to the characteristics of severe source terms under discussion within Phase B [51]. The amount of radioactive material released should involve the risk of early fatalities and should also involve the possibility that changes of wind direction occur during the release

due to its long duration. In the following text it will be referred to as the COMP1 source term. The emission was divided into five hourly phases starting 4,5,7,9, and 16 hours after the accident, respectively. The core inventory was the same as for the the reference plant Biblis, Reactor Unit B of the German Risk Study - Phase A [2]. Figure 11 indicates the temporal characteristics of the chosen source term.

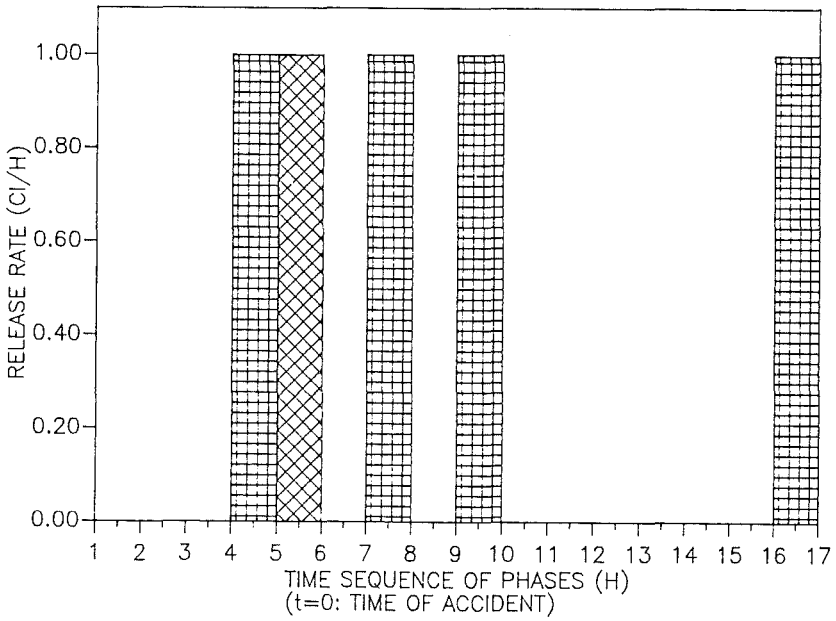

Figure 11. Temporal behaviour of artificial source term COMP1: the duration of each phase is one hour

Phase	Released fractions of core inventory									
	Xe-Kr	J	Cs-Rb	Te-Sb	Ba-Sr	Ru [1]	La [2]	Rel. fractions of forms of iodine [3]		
1	0.0	5.0E-2	5.0E-2	2.5E-2	5.0E-4	5.0E-7	5.0E-5	0.0	0.0	1.0
2	0.0	1.0E-2	1.0E-2	5.5E-3	1.0E-4	1.0E-7	1.0E-5	0.0	0.0	1.0
3	0.0	1.0E-2	1.0E-2	5.5E-3	1.0E-4	1.0E-7	1.0E-5	0.0	0.0	1.0
4	0.0	2.5E-3	2.5E-3	1.25E-3	2.5E-5	2.5E-8	2.5E-6	0.0	0.0	1.0
5	0.0	2.5E-3	2.5E-3	1.25E-3	2.5E-5	2.5E-8	2.5E-6	0.0	0.0	1.0

Table 11. Source term COMP1: Released fractions of core inventory:
[1] including Rh, Co, Mo, Tc
[2] including Y, Zr, Nb, Ce, Pr, Nd, Np, Pu, Am, Cm
[3] iodine group divided according to the chemical form in elemental/organic and particulate constitutents

Table 11 gives the fractions of core inventory released. Noble gases have not been considered at all. The reason is that they contribute to radiation doses due to external exposure to γ-radiation from the passing cloud and the model TRANSLOC has no sub-

model to take into account γ-radiation. Table 11 also indicates that all iodine has been released in particulate form. There are two reasons for this assumption. To consider only one physico-chemical form of the released material reduces the computational effort considerably, especially for TRANSLOC and RIMPUFF. Secondly, it was not the aim to give quantitative assessments of the consequences following a postulated accident scenario; for this purpose the consideration of different physico-chemical forms of nuclides would be of importance because their deposition properties are different. But a qualitative and quantitative comparison of different atmospheric dispersion and deposition models on the basis of probabilistic accident consequences will not loose generality if no distinction is made between gaseous and particulate effluents.

By that time when the decision for the new COMP1 source term had been made, the meteorological input data for RIMPUFF and TRANSLOC had been already prepared by the RISO National Laboratory and the Battelle Institute, respectively, according to the modified FK2 release shown in Figure 10. Because both models had not been developed for the application in ACAs but only for the simulation of single atmospheric dispersion and deposition cases, a change of the source term characteristic was synonymous with the preparation of completely new meteorological input data sequences which would have been an awful lot of work. Therefore, a further source term had been constructed, referred to as COMP2, which is a combination of the modified FK2 release (Figure 10) and the COMP1 source term. The release is divided into three consecutive hourly phases starting 4,5,and 6 hours after the accident. Thus it resembles the modified FK2 source term with respect to the temporal behaviour of the first three release phases; the fourth phase has been omitted and the starting time of the first phase has been shifted by 3 hours. The total fraction of the core inventory released is the same as for the COMP1 source term (Table 11) but now uniformly distributed over the three consecutive release phases for each nuclide group. The temporal characteristic of the COMP2 source term and the corresponding fractions of core inventory released are illustrated in Figure 12 and Table 12, respectively.

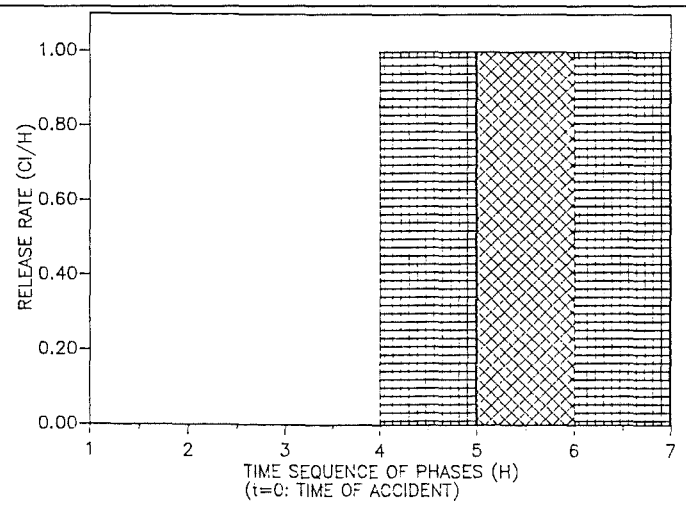

Figure 12. Temporal behaviour of artificial source term COMP2: the duration of each phase is one hour

Phase	Released fractions of core inventory									
	Xe-Kr	J	Cs-Rb	Te-Sb	Ba-Sr	Ru [1]	La [2]	Rel. fractions of forms of iodine [3]		
1	0.0	2.5E-2	2.5E-2	1.25E-2	2.5E-4	2.5E-7	2.5E-5	0.0	0.0	1.0
2	0.0	2.5E-2	2.5E-2	1.25E-2	2.5E-4	2.5E-7	2.5E-5	0.0	0.0	1.0
3	0.0	2.5E-2	2.5E-2	1.25E-2	2.5E-4	2.5E-7	2.5E-5	0.0	0.0	1.0

Table 12. Source term COMP2: Released fractions of core inventory:
[1] including Rh, Co, Mo, Tc
[2] including Y, Zr, Nb, Ce, Pr, Nd, Np, Pu, Am, Cm
[3] iodine group divided according to the chemical form in elemental/organic and particulate constitutents

3.3 *Benchmark tasks*

In Chapter 2 the basic differences between the straight-line Gaussian model and the trajectory models and the different physical concepts of the improved models have been described. On the basis of these differences the following benchmark tasks have been formulated:

1. to study the influence of changes of wind direction on ACA results the model MUSEMET is applied as a conventional straight-line Gaussian model and as a trajectory model. Using the same model ensured that only the trajectory concept might have implications on the accident consequences. A straight-line model offers two possible modes of application:

   a. dispersing the released material in an arbitrary but fixed downwind direction (in the following text referred to as mode 2);
   b. dispersing the released material into the downwind direction prevailing in the first hour of each phase of the release and keeping this direction constant throughout the phase (referred to as mode 3).

   Both modes will be considered and compared with the trajectory mode (referred to as mode 1) which represents the most realistic case taking into account changes of wind direction during the release and the dispersion. The differences between the three modes of application are illustrated schematically in Figure 13 for a multiple phase release. In analogy to the German Risk Study - Phase A the calculations are carried out up to a source distance of 450 km which corresponds to an outer radius for dose calculations of 540 km. The meteorological data of only one single station, namely Frankfurt/Airport, which has been considered representative for the plant location and the area over which the material is dispersing, has been taken into account. For MUSEMET these meteorological data are available in a convenient form which allows to consider any source term with arbitrary temporal characteristics. Therefore, the change from the modified FK2 to the COMP1 source term had no consequences for the application of MUSEMET and this benchmark task could be performed on the basis of the COMP1 release which involves a high probability of

changes of wind direction during the release due to its long duration. All 95 weather sequences described in Section 3.1 have been considered.

2. To investigate the difference between the segmented plume, the multiple puff and the three-dimensional Eulerian grid model the models MUSEMET, RIMPUFF and TRANSLOC have been applied as trajectory models. Initially, this task has been designed to study the influence of a numerical model like TRANSLOC on the ACA results in the near-to-the-site region. Therefore, the calculations are carried out only up to a source distance of 20 km with a corresponding outer radius for dose calculations of 22 km. Since there is only one meteorological station located in the 20 km circle around the source site, namely Frankfurt/Airport, again only the data of this single station are used. This benchmark task has been based on the COMP2 source term. Because the probability of pronounced changes of wind direction during the three consecutive releases is not very high it was the principal intention of task 2 to study the implications of different modelling concepts. Only the 48 "summer" weather sequences with precipitation data have been used for this comparison. The reason why not all 95 sequences have been considered is similar as for the introduction of the COMP2 source term. Because the preparation of the meteorological input data would have been an elaborate work (95 different data groups for 95 sequences) the RISO National Laboratory asked to reduce the number of weather sequences to the 48 "summer" cases.

3. The influence of inhomogeneous meteorological flow, precipitation and stability fields has been investigated. For this purpose the dispersion calculations along wind fields have been carried out up to source distance of 200 km around the site using the RIMPUFF model. Meteorological data are taken from eight stations which have hourly recordings for wind speed and wind direction (Figure 14). For each station the model also needs hourly informations on stability and precipitation intensity. As not all of the stations chosen have recordings of these parameters, it was necessary to associate informations from nearby stations [46]. Table 13 indicates that the stability is mainly governed by the stations Frankfurt, Saarbrücken and Stuttgart. Because of the low density of meteorological stations in the 200 km area around the source it is obvious that the influence which topography has on the atmospheric fields cannot be represented. Therefore, it has to be assumed that the topography over which the dispersion is modelled is uniform. The corresponding calculations assuming homogeneous atmospheric conditions during hourly time intervals were performed with the segmented plume model MUSEMET. They have been based again on the hourly changing meteorological data of Frankfurt/Airport. Again only the 48 "summer" sequences have been considered to estimate the consequences following the COMP2 release.

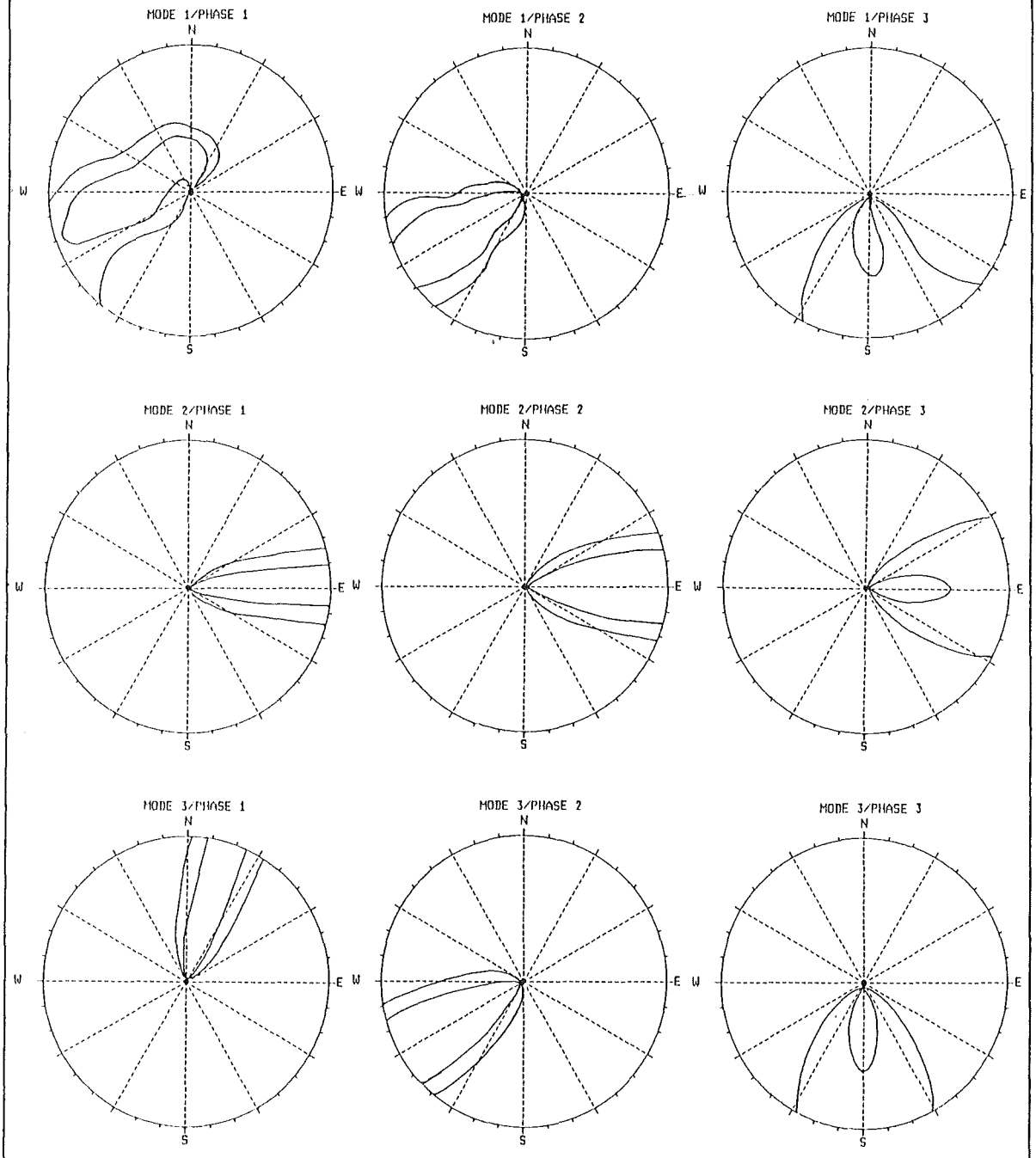

Figure 13. Illustration of modes of application of a Gaussian model: explanation of modes see text

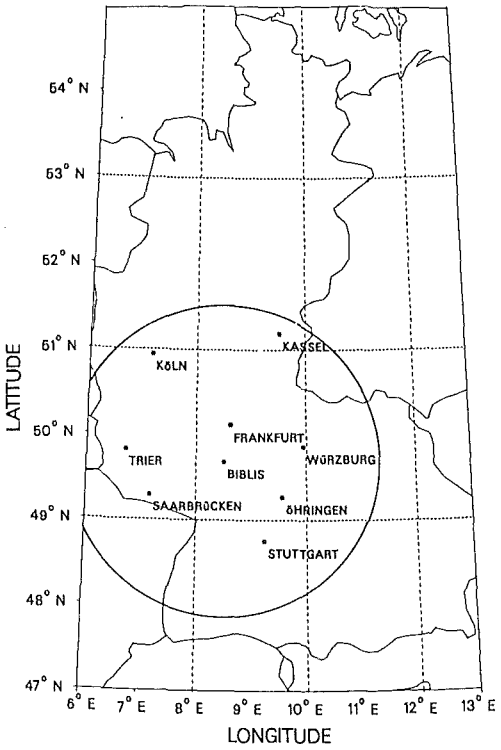

Figure 14. Map of the area covered by the dispersion modelling: geographical positions of meteorological stations and of the source site are indicated

Station Name	Data for		
	Wind	Stability	Precipitation Intensity
	are taken from		
Frankfurt	Frankfurt	Frankfurt	Frankfurt
Würzburg	Würzburg	Stuttgart	Würzburg
Stuttgart	Stuttgart	Stuttgart	(Freiburg + Würzburg)/2 [1]
Öhringen	Öhringen	Stuttgart	Würzburg
Saarbrücken	Saarbrücken	Saarbrücken	(Freiburg + Frankfurt)/2 [1]
Trier	Trier	Saarbrücken	Frankfurt
Köln	Köln	Köln	Frankfurt
Kassel	Kassel	Frankfurt	Frankfurt

Table 13. Meteorological stations used in benchmark task 3: Calculations with RIMPUFF
[1] Mean value of precipitation intensity for the 2 stations

Assuming a unit release for each release phase, each atmospheric dispersion model calculated normalized time-integrated air concentration and ground contamination patterns. In addition, the arrival time of the radioactive plume at a certain grid element was determined. The spatial normalized concentrations fields and the arrival times were used as input to UFOMOD to calculate the initial air and ground activity concentrations of individual radionuclides at each grid point according to the source term and to correct for radioactive decay during dispersion. Then UFOMOD optionally calculated distribution functions of air concentration, contaminated ares, organ doses and health effects of individuals and in the population together with areas and the number of persons affected by countermeasures.

3.4 Computational effort

The three models, MUSEMET, RIMPUFF, and TRANSLOC and their corresponding meteorological input data have been transferred to KfK and implemented on the KfK computer system at the beginning of the study

1. to get a better understanding of the structure of each model which was essential to carry out model modifications necessary for the application in ACAs;

2. to test the models with respect to physical and programming errors;

3. to carry out most of the computer runs necessary for the comparative study.

The atmospheric dispersion model used in UFOMOD should fulfill some basic requirements with regard to its program structure.

- The model must be able to consider a rather large amount of different dispersion situations (weather sequences) which can be divided each into several release phases. This implies that the meteorological input data are available in a convenient form. Commonly, the weather sequences overlap with respect to time and therefore, an organization of the meteorological data which allows a direct access would be preferable to a sequential data set organization.

- To avoid several restarts of the model it should be able to consider several types of nuclides with different dry and wet deposition properties during one computer run.

- The values of time-integrated air and ground-level concentrations have to be available on a polar grid with the centre point at the location of the nuclear facility. The radial and azimuthal resolution have to be variable so that the polar grid can be selected rather fine in the vicinity of the source but more rough at larger distances.

Nearly no modification had to be made in the model MUSEMET because it has been developed intentionally for the application in ACAs and therefore, all requirements mentioned were fulfilled. Only a simple interface has been built to transfer the MUSEMET results to UFOMOD.

Index of hor. grid elements grid distance (m)	1 2000	2 2000	3 2000	4 2000	5 2000	6 1000	7 1000	8 1000
Index of hor. grid elements grid distance (m)	9 1000	10 1000	11 1000	12 500	13 500	14 500	15 500	16 300
Index of hor. grid elements grid distance (m)	17 300	18 200	19 200	20 200	21 200	22 200	23 100	24 100
Index of hor. grid elements grid distance (m)	25 100	26 100	27 100	28 100	29 100	30 200	31 200	32 200
Index of hor. grid elements grid distance (m)	33 200	34 200	35 300	36 300	37 500	38 500	39 500	40 500
Index of hor. grid elements grid distance (m)	41 1000	42 1000	43 1000	44 1000	45 1000	46 1000	47 2000	48 2000
Index of hor. grid elements grid distance (m)	49 2000	50 2000	51 2000					
Index of vert. grid elements grid distance (m)	1 1	2 1	3 2	4 4	5 7	6 10	7 10	8 15
Index of vert. grid elements grid distance (m)	9 20	10 30	11 20	12 20	13 20	14 40	15 50	16 50
Index of vert. grid elements grid distance (m)	17 50	18 50						

Table 14. Horizontal and vertical grid resolution of TRANSLOC

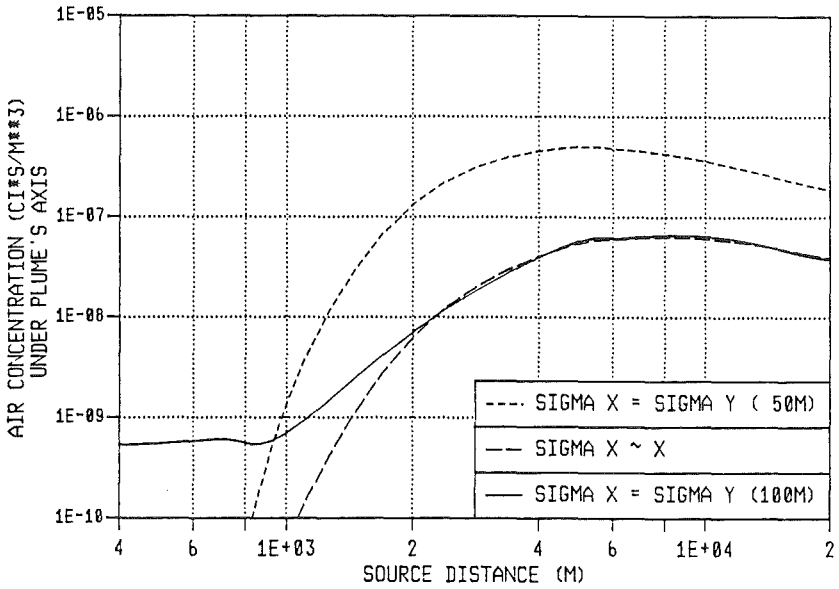

Figure 15. Illustration of "backward diffusion" in MUSEMET: release height: H = 100m stability category: F

The RIMPUFF model has been designed for atmospheric dispersion and deposition studies of single cases. Most of the necessary modifications described above could be made with some programming effort, including the implementation of an interface to UFOMOD. Only the structure of the meteorological input data set has not been improved in the beginning of the study. Therefore, it was necessary to create a new sequentially organized data set for each weather sequence which made the preparation very uncomfortable. In the meantime, during a general review and revision of RIMPUFF with respect to programming techniques carried out together with the Gesellschaft für Reaktorsicherheit (GRS), Cologne [52], the structure of the meteorological data sets has been changed to a more convenient form similar to that of MUSEMET [53]. After this revision it was possible to run RIMPUFF very effectively on the vector processor FUJITSU-VP50 installed at KfK.

Because of the high CPU-time required by TRANSLOC it was useless to consider more than one type of nuclide during one run, and it was also not possible to introduce a polar concentration grid. The model has been modified to take into account several weather sequences with several phases. But by reason of high CPU-time the dispersion and deposition simulations have to be terminated at latest five hours after the beginning of a phase assuming that after that time most of the activity has been deposited and that the remaining airborne material does not contribute essentially to the air and ground-level concentrations. In contrast, the only condition in RIMPUFF and MUSEMET to stop the atmospheric dispersion calculation is that the last puff or the plume must have left the predefined area over which the activity is dispersing. But TRANSLOC could be improved in two other points. Firstly, the equidistant horizontal grid size was changed to a non-equidistant, variable one, thus ensuring that the concentration distributions could be calculated with a sufficient high resolution in the environment of the source. The grid distances varied from 100m in the immediate neighbourhood of the source to 2000m at the outer edge of the predefined area (Table 14). By this change it was possible in a data transfer interface to perform an interpolation of the TRANSLOC results from the rectangular grid to the required polar grid using bi-cubic splines.

Secondly, a procedure was developed to consider short-term fluctuations of the horizontal wind direction [45] although only hourly meteorological data have been available. Based on 10-minute averages of measured fluctuations of the horizontal wind direction, variations of the hourly mean wind direction are calculated randomly for each time-step.

Concurrently with the modifications the models have been tested to check the changes and to look for physical and programming errors. Essentially, the errors detected and corrected were programming errors. In RIMPUFF the explicit modelling of the multiple reflection at an upper inversion layer had to be changed because it is only valid if the activity is not distributed uniformly over the whole mixing layer which is assumed to be limited by the inversion layer. Keeping this modelling would result in ground concentration values at far distances from the source which are too high relative to the air concentrations in the same distance ranges. Therefore, the reflection at the inversion has been parameterized by limiting the vertical dispersion parameter σ_z as described in Section 2.7. Additionally, one effect in the MUSEMET results which has been formerly explained as "longitudinal backward diffusion" could be clarified. Under certain circumstances unrealistic high concentration values were observed near to the source in the the

downwind direction and even in the upwind direction from the source. This is illustrated by the full line in Figure 15 which show the normalized time-integrated air concentration near to the ground under the axis of a straight-line Gaussian plume resulting from a unit release at a height of 100m under stable atmospheric conditions. In similar situations but with changes of wind direction the areas contaminated with high concentration values increased considerably. Test calculations revealed that this effect was a numerical "backward diffusion" as a result of the parameterization $\sigma_x = \sigma_y$ inherent in the factor Δf_n of Eq. (2.9) which, in contradiction to one of the basic assumptions of the Gaussian model, might lead to a predominance of the turbulent downwind diffusion compared to the advection by the mean wind. Especially, together with the use of dispersion parameter sets which show rather high values, this unrealistic effect became dominant. In this study the Karlsruhe-Jülich-System (Table 2) should have been applied which show very large numbers of σ_y at release heights $\geq$ 100m because they comprise low-frequency meandering of the horizontal wind during very stable atmospheric conditions [24]. To overcome this problem, Geiß [54] proposed not to change the assumption $\sigma_x = \sigma_y$ but to relate σ_x to short-term (e.g. 10-minute averaged) standard deviations σ_θ of the horizontal wind direction. Therefore, σ_x has been parameterized as

$$\sigma_x = \frac{2}{3} \, x \, \tan \sigma_\theta \qquad (3.1)$$

Typical values of σ_θ (Table 15) are available from measurements at the nuclear research centres in Jülich and Karlsruhe at heights of 50m and 100m, respectively [55], [56].

Diffusion category	Standard deviations σ_θ of horizontal wind direction (degree)	
	50m height	100m height
A	23.8	20.5
B	18.9	13.9
C	15.3	10.1
D	12.6	6.9
E	10.2	4.0
F	8.6	2.0

Table 15. Standard deviations of horizontal wind direction (degree)

But it should be noticed that the linear increase of σ_x with source distance x (or travel time t) is only valid if the travel time of the plume is smaller than the Lagrangian turbulence time scale [9]. With increasing travel time the rate of diffusion decreases to

$$\sigma_x = \sigma_y \sim \sqrt{t} \sim \sqrt{x}$$

which also comes out from the assumption of Fickian diffusion for the Gaussian model (see Eq. (2.4)). Thus, for larger travel times Eq. (3.1) also led to an unrealistic overestimation of the turbulent downwind diffusion and the corresponding σ_x-values even

became higher than the σ_y parameters determined from dispersion experiments. In such cases the experimental σ_y values were again used for σ_x. The long-dashed line in Figure 15 shows as an example the result of the σ_x parameterization described above. It is evident that the "backward diffusion" vanishes and that the concentration distribution becomes more realistic.

Principally, the same problem appeared in RIMPUFF. But for this model it is required to use the same values for σ_x and σ_y because the horizontal projection of each puff has to be circular to ensure overlapping of the puffs. Therefore, a modelling of σ_x as in MUSEMET was not possible.

Thus, after the identification of the σ_x parameterization problem and due to the lack of a satisfactory physical solution, it has been decided only to use the 50m dispersion parameters of the Karlsruhe-Jülich-System (Table 2) in all calculations with the Gaussian-like regardless of the effective release height. With these parameters the "backward diffusion" problem did not appear (see Figure 15 short-dashed line) and, therefore could not cover and falsify the implications which different concepts of atmospheric dispersion modelling might have on the probabilistic ACA results.

At the end of the test phase programming errors were not evident anymore and also the physics included in the models seemed to work realistically.

The last computational step then was to carry out the calculations for the three benchmark tasks. Most of these have been performed on the Siemens M7890 computer at KfK. Only the calculation of concentration distribution for particulate material with TRANSLOC were carried out by the Battelle Institute, Frankfurt, itself, and the results were transferred to KfK. But to get a comparable indication of the CPU-time required by a numerical grid model, TRANSLOC runs for gaseous radioactive releases according to benchmark task 2 have been performed also on the KfK M7890 system. Additionally, all RIMPUFF calculations have been repeated on the vector processor VP50 after the structural revision of the program to get an impression of the performance of the vectorized version compared to the scalar one. It is obvious that the CPU-time required by each model strongly depends on the mode of application: on the number of weather sequences, the number of different nuclide types, the size of the area over which material is dispersing, the number of puffs released, and the meteorological conditions. The last one is the most uncertain factor in predetermining the required CPU-time because, in principle, it is not known in advance how long a plume or a number of puffs remain over a predefined area because this residence time strongly depends on the prevailing wind conditions.

The Tables 15 to 17 summarize the characteristics and computational conditions of benchmark tasks 1 to 3, respectively, also indicating the computational size of each task.

The total CPU-time the trajectory mode of MUSEMET required for benchmark task 1 was about 20 min (Table 16). This was an increase in CPU-time of a factor of five compared to the two straight-line Gaussian modes which needed of course the same CPU-time.

Participating model	MUSEMET, with different modes of application • trajectory mode (mode 1) • straight-line Gaussian mode with arbitrary but fixed wind direction (mode 2) • straight-line Gaussian mode taking into account the initial wind direction of each release phase (mode 3)		
Source term	COMP1		
Release height	10m, no plume rise		
No. of weather sequences	95, each divided into 5 hourly release phases		
Meteorological data	hourly data of wind speed, wind direction, Pasquill-Gifford stability category and precipitation of Frankfurt/Airport		
Maximum source distance	450 km		
Radial source distances (m)	700, 1000, 1400, 2000, 3000, 4500, 6700, 10000, 14000, 20000, 30000, 45000, 67000, 100000, 140000, 200000, 300000, 450000		
Azimuthal resolution	5°		
No. of polar grid points considered	1296		
CPU-time required (min)	Mode 1	Mode 2	Mode 3
	20	4	4

Table 16. Summary of computational conditions of benchmark task 1

For benchmark task 2 the differences in CPU-time were striking (Table 17). While MUSEMET managed this task in about one minute, RIMPUFF needed four hours on the scalar processor M7890. It should be noted that the CPU-time required by RIMPUFF strongly depends on the number of puffs released and the number of advection steps for each puff. For example, a reduction of both numbers by a factor of two, if possible, would reduce the CPU-time by nearly a factor of four. The use of the vector processor VP50 decreased the required computer time for RIMPUFF by a factor of six. About 81% of the total CPU-time the program spent on the vector unit of the VP50 indicating that the vectorization grade of the revised RIMPUFF version is more than 95%. But it should be noticed that this is only valid for the VP50 vector processor. The unacceptable CPU-time of about 24 hours for TRANSLOC revealed that atmospheric dispersion models like TRANSLOC cannot be used generally in ACAs.

For benchmark task 3 MUSEMET needed about two minutes while RIMPUFF required 90 minutes CPU-time on the scalar processor (Table 18). The use of the vector machine reduced the total CPU-time for RIMPUFF to 13 minutes. Nine minutes of this time the program spent on the vector unit. Although the maximum source distance of 200km was a factor of 10 larger, RIMPUFF needed less CPU-time than in task 2 because the puff fre-

quency had been decreased from 60 puffs/h to 20 puffs/h, and the time step for puff advection had been increased from 30 sec to 180 sec.

Participating models	MUSEMET, RIMPUFF, TRANSLOC as trajectory models			
Source term	COMP2			
Release height	20m + plume rise according to Table 6			
No. of weather sequences	48, each divided into 3 consecutive hourly release phases			
Meteorological data	hourly data of wind speed, wind direction, Pasquill-Gifford stability category and precipitation of Frankfurt/Airport and, in addition, vertical temperature profiles measured twice daily at stations Essen and Stuttgart			
Maximum source distance	20 km			
Radial source distances (m)	300, 500, 750, 1000, 1300, 1800, 2400, 4200, 5600, 7500, 10000, 13000, 16000, 20000			
Azimuthal resolution	5°			
No. of polar grid points considered	1080			
grid distance of the RIMPUFF advection grid	1000m			
No. of puffs released in RIMPUFF per hourly release phase	60			
Time step for puff advection	30 sec			
Dimension of TRANSLOC grid	51*51*18; source is located at horizontal position (26,26)			
CPU-time required	MUSEMET	RIMPUFF		TRANSLOC
		scalar	vector	
	1 min	240 min	42 min	24 h

Table 17. Summary of computational conditions of benchmark task 2

To see whether the decrease of puff frequency and numbers of advection intervals also led to reasonable concentration values in the polar grid chosen for task 3 (see Table 18), some test calculations had been peformed. For this purpose a polar grid has been chosen with a combination of the radial distances shown in Table 17 and Table 18 up to a maximum source distance of 45km. A typical result is presented in Figure 16 which shows the normalized air concentrations of Cs-137 under the axis of the plume. The full line represents the results according to the computational conditions of benchmark task 2 (Table 17), and the dashed line represents the results of the test calculation according to task 3 (Table 18) but with the combined polar grid up to 45km.

Participating models	MUSEMET, RIMPUFF, as trajectory models		
Source term	COMP2		
Release height	20m + plume rise according to Table 6		
No. of weather sequences	48, each divided into 3 consecutive hourly release phases		
Meteorological data	hourly data of wind speed, wind direction, Pasquill-Gifford stability category and precipitation of 8 meteorological stations (Table 13)		
Maximum source distance	200 km		
Radial source distances (m)	4500, 6700, 10000, 14000, 20000, 30000, 45000, 67000, 100000, 140000, 200000		
Azimuthal resolution	5°		
No. of polar grid points considered	792		
grid distance of the RIMPUFF advection grid	20 km		
No. of puffs released in RIMPUFF per hourly release phase	20		
Time step for puff advection	180sec		
CPU-time required (min)	MUSEMET	RIMPUFF	
		scalar	vector
	2	90	13

Table 18. Summary of computational conditions of benchmark task 3

Figure 16 demonstrates that the puff frequency and advection time intervals chosen for benchmark task3 lead to unreasonable results if a polar grid with a rather high resolution in the near range is considered. But beyond 4.5km which is the first radius considered in task3 and where the distance between adjacent radii increases from a few hundred of meters to kilometres, both curves agree perfectly. Therefore, there is no need to perform the RIMPUFF calculations of benchmark taks 3 with a puff frequency and a number of advection time steps as high as in task 2 in order to get reliable concentration distributions.

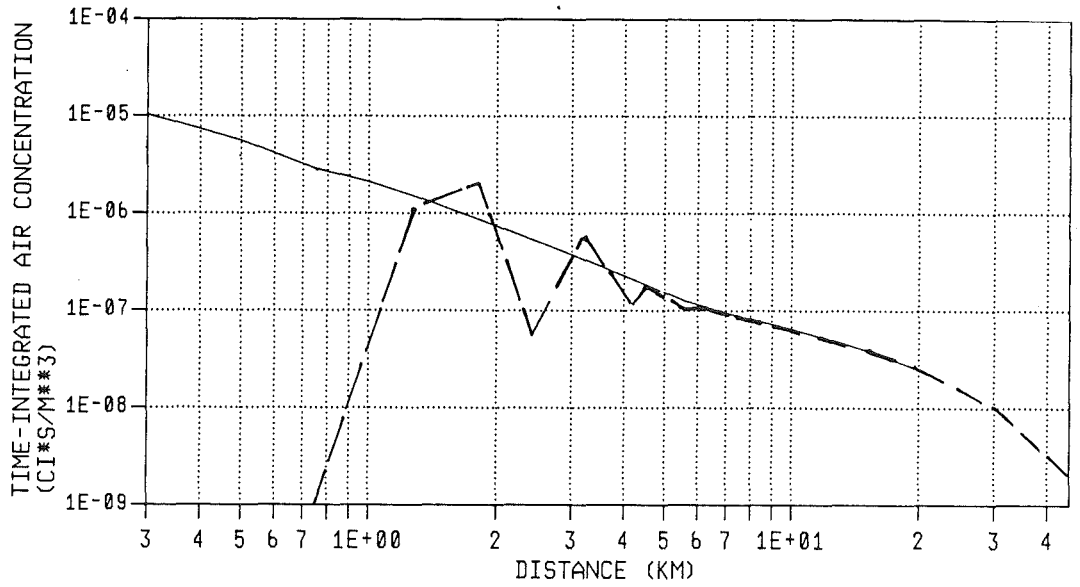

Figure 16. Influence of puff frequency, number of advection intervals, and polar grid size on RIMPUFF results:
full line: conditions according to benchmark 2 (Table 17)
dashed line: test calculation (see text)

In the following chapter examples of different types of accident consequences are shown for each benchmark task to compare the results with respect to the different concepts of atmospheric dispersion modelling.

4. RESULTS OF THE COMPARISONS

4.1 Influence of changes of wind direction

The purpose of the first benchmark task (see Sect. 3.3) was to study the implications which changes of wind direction during the release and the dispersion might have on the results of accident consequence assessments. Therefore, the model MUSEMET was applied with three different modes (Figure 13).

The application in the trajectory mode (mode 1) has obviously two principle consequences.

- Firstly, an increase of the size of the areas over which the radionuclides are distributed (Figure 17).
- Secondly, a prolongation of the time period the trajectory plume needs to leave a certain distance range (Figure 18).

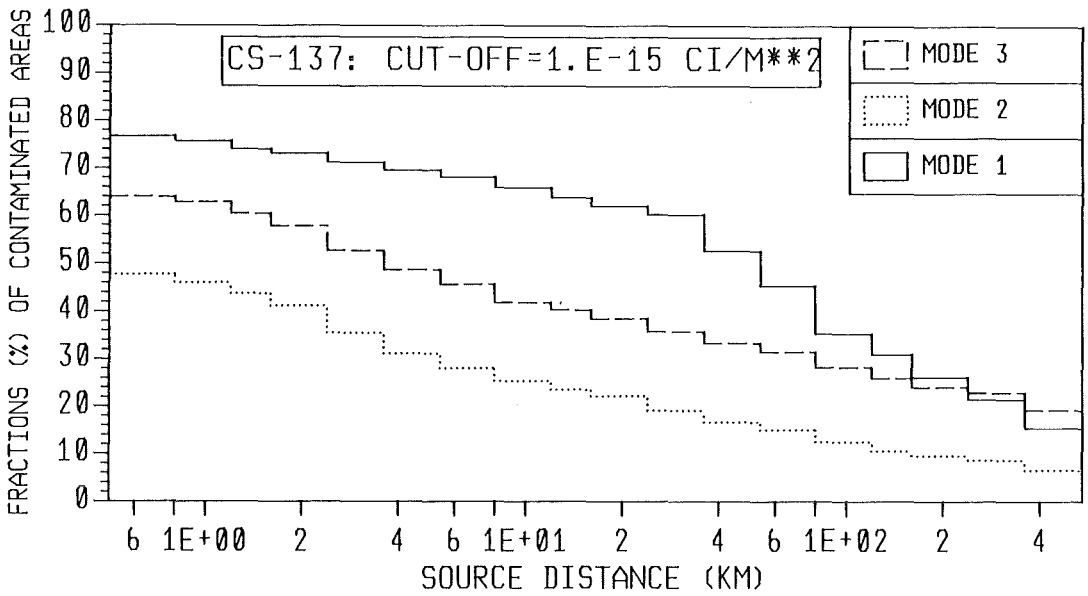

Figure 17. Mean relative size (%) of areas affected by different model modes: nuclide considered: CS-137

Figure 17 indicates the spatial distribution of activity by the three different model versions. It is expressed as the mean size of contaminated areas in different distance bands relative to the size of the whole corresponding circular ring. Therefore, each curve in Figure 17 indicates the probabilities that in certain distance ranges a contamination above the cut-off occurs anyhow. The mean areas are averaged over all weather sequences. The radial extension of each ring is indicated by the length of the horizontal bars of the step functions . The lower boundary of the first band is 0 m, the upper boundary of the last one is 540 km. It has to be noticed that only those areas have been con-

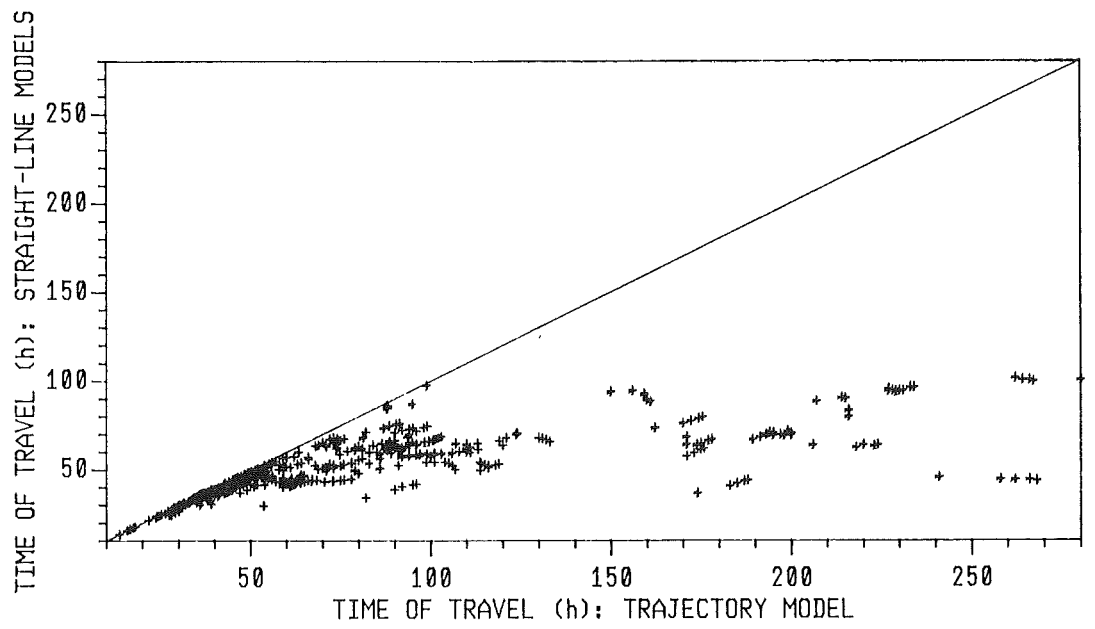

Figure 18. Travel times (h) of plumes to leave a 450 km circle around the source

sidered which are contaminated with activity concentrations above a certain cut-off concentration. Such a cut-off can be defined in MUSEMET as a fixed value. In the case of benchmark task 1 it had been set to $C_{cut}^{air} = 10^{-12}$ (Ci s m^{-3}) for the normalized time-integrated air concentration and, thus, to $C_{cut}^{gr} = C_{cut}^{air} v_d + C_w$ (Ci m^{-2}) for the ground concentration.

From Figure 17 it can be concluded that the consideration of changes of wind direction during the release (mode 1 and 3) and during the dispersion (only mode 1) leads to a considerably larger distribution of activity than the conventional straight-line model (type 2).

The figure indicates a pronounced distance dependence of the sizes of areas affected by the trajectory model relative to the straight-line model versions. Regarding the two straight-line models, the atmospheric dispersion conditions are exactly the same in all distances. Therefore, no differences exist between these two model types with respect to travelling time, deposition properties, and turbulent dilution of radioactive plumes. The only difference is the consideration of changes of wind direction during the release leading to a nearly constant increase of contaminated areas in all distances if the mode 3 model version is used.

With respect to the trajectory model Figure 17 shows an increase of contaminated areas relative to the straight-line model versions up to intermediate distance ranges. In farther distances the difference decreases and even might become negative. It is obvious that due to the consideration of changes of wind direction during the release and the transport the activity will be distributed over larger areas. Additionally, as it is shown in Figure 18, the times the trajectory plumes need to leave the whole dispersion area and, thus, also the effective distances they travel may increase considerably.

By these reasons a larger amount of activity can be deposited over larger areas by dry deposition and wash-out, especially in the regions near to the source, where the plumes still contain most of the released activity. Therefore, the increase of contaminated areas relative to the straight-line models can be observed.

On the other hand, the trajectory plumes are depleted more effectively by the augmented deposition so that they contain a smaller amount of restactivity when they finally leave the dispersion area (Figure 19).

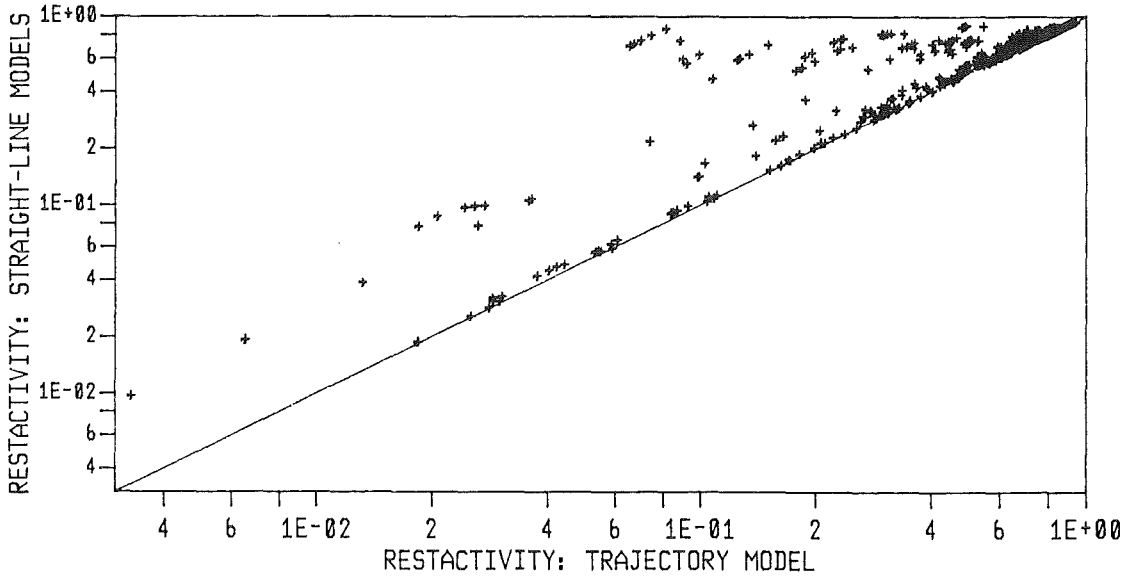

Figure 19. Restactivities in the plumes when they leave a 450 km circle: Figures on axes are fractions of an unit release of CS-137

In addition, the trajectory plumes are much more diluted due to their dispersion along the longer ways. Therefore, the sizes of areas in the far distance ranges with concentrations above the cut-off must decrease relative to the straight-line modes. Even if only non-depositing noble gases are considered the effect becomes evident. This emphasizes the role of increased dispersion along the trajectories.

The most comprehensive representation of the variation of accident consequences caused by the different weather sequences considered and the azimuthal distribution of radioactive material are **c**omplementary **c**umulative **f**requency **d**istribution (CCFD) functions in different distance bands. As a typical example, Figure 20 shows the CCFDs of Cs-137 concentrations on the ground surface estimated in two radial distance bands by the three different dispersion models.
The CCFD curves give the expected frequency that a certain concentration level is reached or exceeded assuming the release has occurred. From Figure 20 it can be deduced that the frequencies of occurrence of smaller concentrations are greater if changes of wind direction are taken into account. This indicates that the activity is distributed over larger areas as it could already be seen in Figure 17. The spatial distribution is largest for the trajectory model in nearly all distances but keeping in mind that

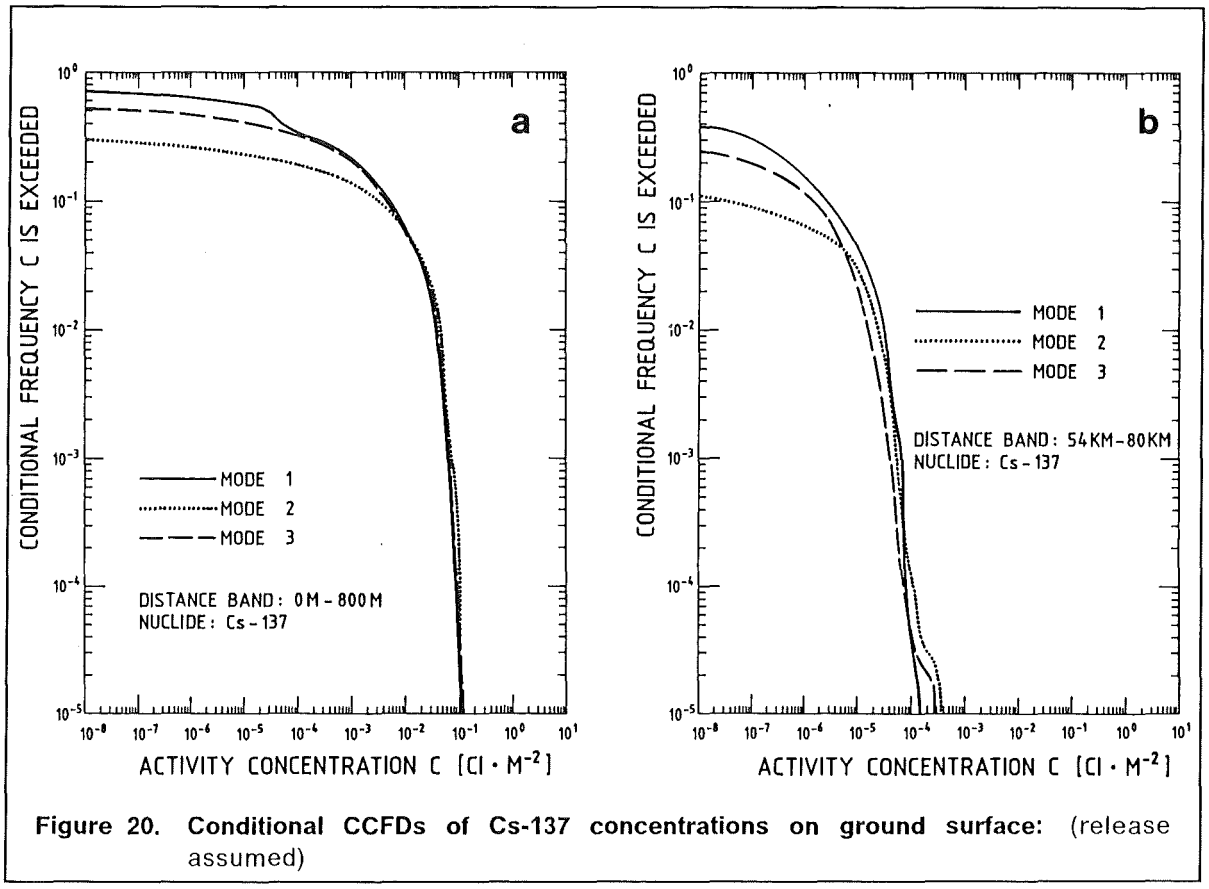

Figure 20. Conditional CCFDs of Cs-137 concentrations on ground surface: (release assumed)

the differences between the models also depend on the concentration cut-off value chosen.

Whilst in the regions near to the site there hardly exists any difference between the three models with respect to higher concentration levels, a reduction of peak level concentrations becomes evident with increasing source distance if changes of wind direction are considered. The good agreement in the neighbourhood of the source might be a combination of meteorological and source term conditions. Due to the temporal behaviour of the COMP1 source term (Figure 11) a persistency of the initial wind directions during the initial stages of those few weather sequences which cause the maximum concentrations cannot be excluded. In such cases the major parts of the released activity (Table 11) would be transported initially in the same direction, and since all other meteorological conditions are also the same in the beginning of each release phase nearly the same high concentration levels should result for all three dispersion models. In farther distances a reduction of the high concentrations calculated with the trajectory model (Figure 20b) is to be expected by reasons of mass conservation because the same amount of activity as for the straight-line model types will be dispersed and deposited over larger areas. For the straight-line Gaussian models (type 2 and 3) the maximum concentrations agree well also in farther distances. They are caused by the same weather sequence so that the explanation is the same as for the agreement in the regions near to the site: there exists a certain probability of no change of wind direction during the initial phases of the weather sequence when more than 66% (first phase) and

more than 80% (first and second phase) of the core inventory are already released (Table 11).

The space- and time dependent distributions of the radionuclide concentrations determine the radiation doses of individuals and in the population and the need for countermeasures which may be taken to reduce the exposure and thus the health implications (Figure 8). Protective actions considered in UFOMOD version B03 are sheltering, evacuation and relocation, decontamination and food-bans ([2], Figure 8, Figure 9, and Table 8).

It cannot be foreseen how the use of more realistic atmospheric dispersion models influences the protective actions and thus also the expected exposure and the health effects. As it is indicated schematically in Figure 21 the broader spatial distribution of activity flattens the steep gradient of potential doses resulting from the conventional straight-line model but rises the dose levels over larger areas. Now it depends upon the magnitude of the dose intervention level and the source term characteristics whether the size of areas affected by countermeasures increase or decrease. If the potential doses are only slightly higher than the intervention level, smaller areas with countermeasures may arise from the use of the more realistic models (Figure 21a). If protective actions are considered which depend on a quite low intervention criterion like relocation, decontamination and food-bans, things might be reversed; the areas increase (Figure 21b). To which amount the intervention levels are exceeded, of course depends upon the source term, its temporal behaviour, and the amount of activity released.

As an example for the COMP1 source term chosen for this comparison, Figure 22 shows the CCFDs of areas and numbers of people affected by fast relocation. Fast relocation of the population to mitigate early fatalities due to external radiation from the ground deemed to be advisable in areas outside the evacuation area if the acute bone marrow dose is equal or greater than 100 rem ([2], Figure 9, Table 8). Figure 22a indicates that the probability of occurrence of areas affected by fast relocation which are greater than 1km^2 is relatively small. It is even a factor of five smaller if the trajectory model is applied because the dose intervention level is exceeded in smaller areas. Averaged over all weather sequences and azimuthal grid elements the area decreases by a factor of three. Consistent with these results the probability that people have to be relocated soon after the accident is considerably smaller using the trajectory model (Figure 22b). On the average the number of people relocated is three times smaller.

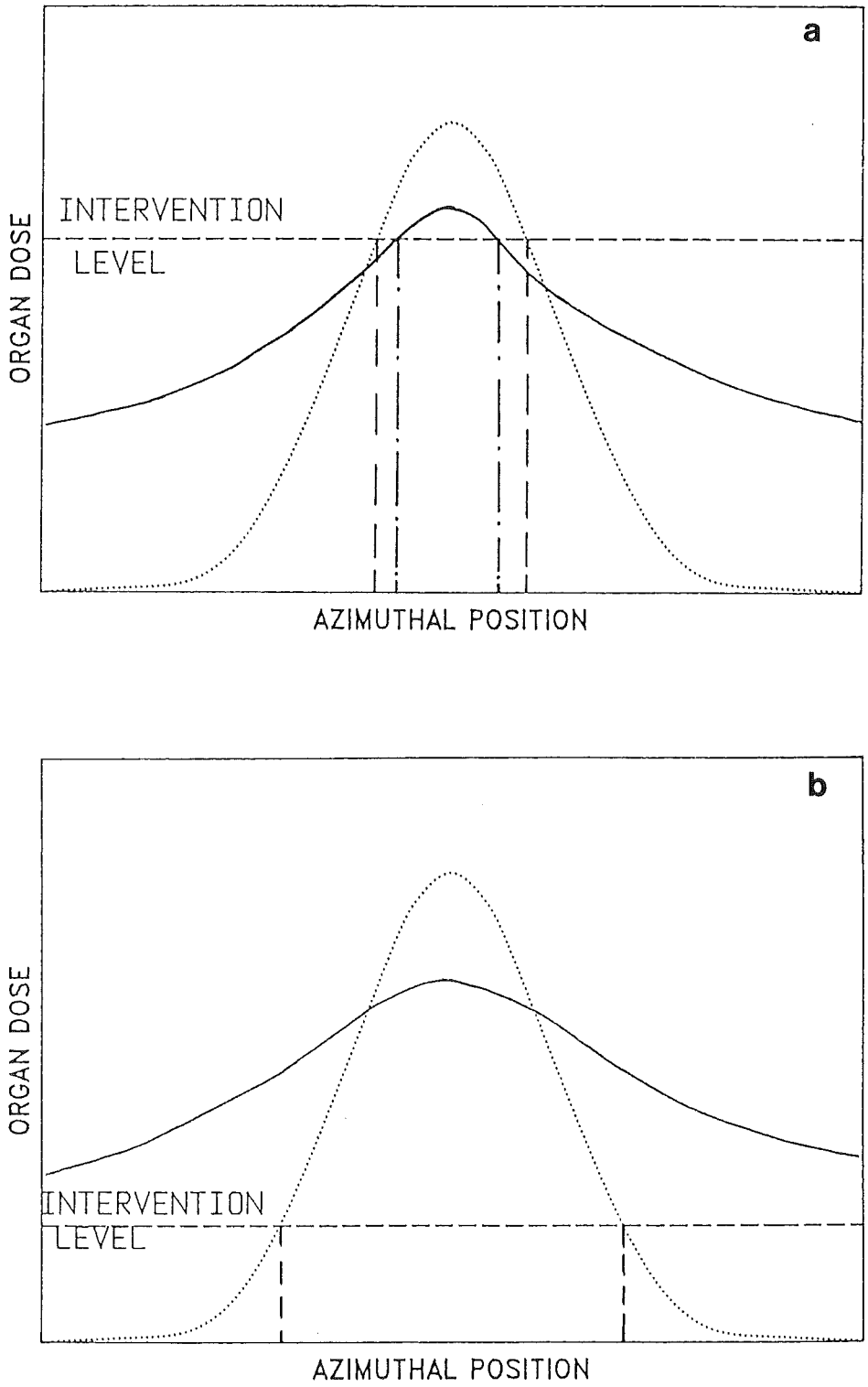

Figure 21. Influence of more realistic atmospheric dispersion models on areas with countermeasures

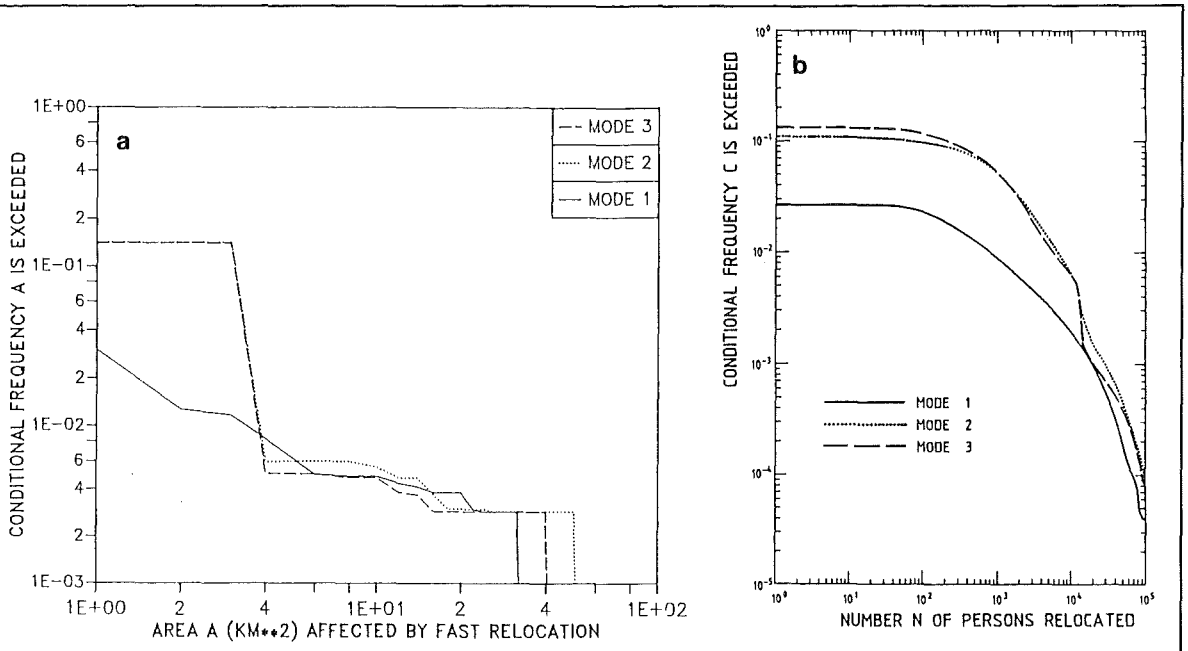

Figure 22. Conditional CCFDs of areas (a) and numbers of people (b) affected by fast relocation: (COMP1 release assumed)

Countermeasures which depend upon low dose criteria and extend over large distances of hundreds and thousands of kilometres like relocation, decontamination, and food-bans are taken to reduce the late somatic and hereditary effects. As an example of the influence the choice of the atmospheric dispersion model might have on these protective actions, Figure 23 shows the corresponding CCFDs of the areas with food-bans of other products than milk in the first year after the accident. It can be seen that under the conditions of the COMP1 source term the size of areas where the consumption and distribution of food should be interdicted increases especially if the trajectory model is applied. For relocation of people and decontamination of land areas the influence of the different atmospheric dispersion models is indifferent and not very much pronounced with regard to the COMP1 source term considered. Using the trajectory model there is a slight tendency that larger areas and thus more people are affected by relocation because the intervention level (250 rem accumulated in the whole body over 30 years, [2]) is exceeded in these areas and, therefore, decontamination cannot be carried out so effectively that the movement of the population can be avoided. Thus, the size of areas to be decontaminated slightly decreases.

But also outside the regions with countermeasures larger contaminated areas appear if changes of wind direction are considered. This can be concluded from Figure 24 which shows that the mean 50-a individual bone marrow doses are higher in all distances if the more realistic models are applied, although countermeasures have already been taken into account. The values are averages over all weather sequences and azimuthal sectors in each distance band. They can be interpreted as the expected exposure an individual experiences at any azimuthal position in the corresponding distance range. In accordance with this result the number of late fatalities increases if changes of wind direction

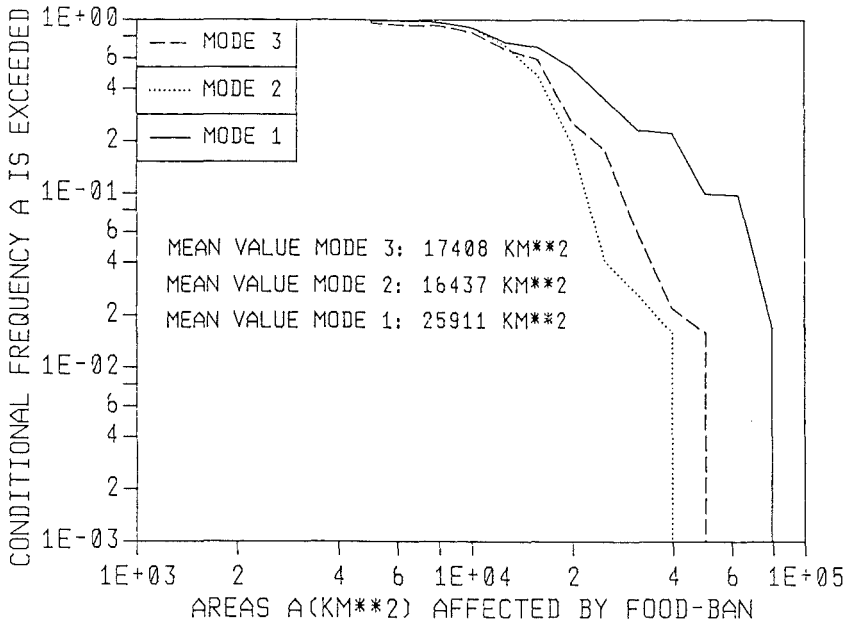

Figure 23. Conditional CCFDs of areas with food-bans execpt milk in the first year: (COMP1 release assumed)

are taken into account. If the trajectory model is applied instead of the conventional straight-line model they are about a factor of two higher.

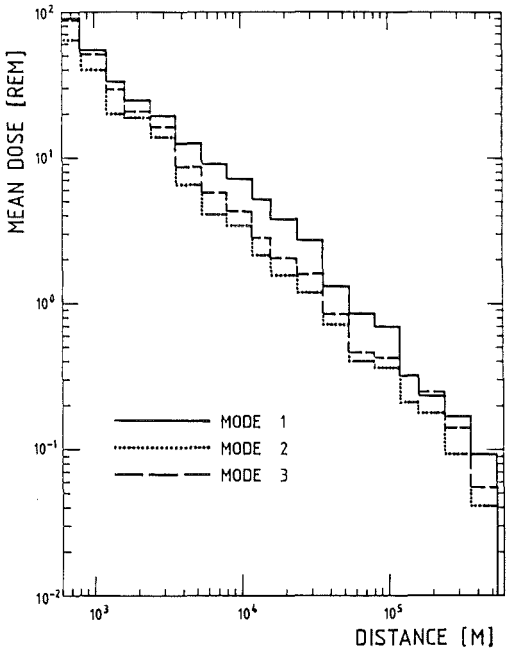

Figure 24. Mean 50-a individual bone marrow doses as functions of distance

In the UFOMOD/B03 version early fatalities arising from a reactor accident are due almost exclusively to the radiation dose absorbed by the bone marrow [2]. If a threshold of 100 rem is exceeded a risk of acute bone marrow syndrom exists. The small probability that early fatalities occur anyhow (4% for the mode 2 version) further decreases to 2.5% for the mode 1 and mode 3 model versions, and also the average number decreases by a factor of two. This indicates that due to the consideration of changes of wind direction during the release less people are exposed to acute doses above the dose-risk threshold.

To summarize this section it can be concluded that the application of the trajectory model leads to

- a spatial distribution of activity over larger areas (Figure 17),
- an increase of radioactive plume's residence time in the area over which it is dispersing (Figure 18),
- enhanced depletion and dilution by dry and wet deposition processes and turbulent diffusion along the longer trajectories (Figure 19).

Generally, it can be stated that the trajectory model provide more realistic results of ACAs than the straight-line Gaussian models because the consideration of changes of wind direction gives a more realistic picture of atmospheric processes as everybody can see observing a smoke plume coming out off a chimney. Dependent on the source term characteristics more or less pronounced differences may arise in the consequences. Especially, longer or shorter release durations will increase or decrease the deviations from the predictions of the conventional straight-line Gaussian plume model.

4.2 Differences between plume, puff, and numerical modelling concepts

The purpose of the second benchmark task (see Sect. 3.3) was to compare the accident consequences resulting from the application of a segmented plume, a multiple puff, and a Eulerian grid model and to relate possible differences to the different modelling concepts. It has been assumed that the COMP2 release has occurred (see Sect. 3.2)

Figure 25 indicates the spatial distribution of activity by the three models. It is expressed as the mean relative size of areas affected by Cs-137 concentrations above a cut-off value. In this case the value was $C^{air}_{cut} = 10^{-15}$ (Ci s m^{-3}) for the air concentration near to the ground.

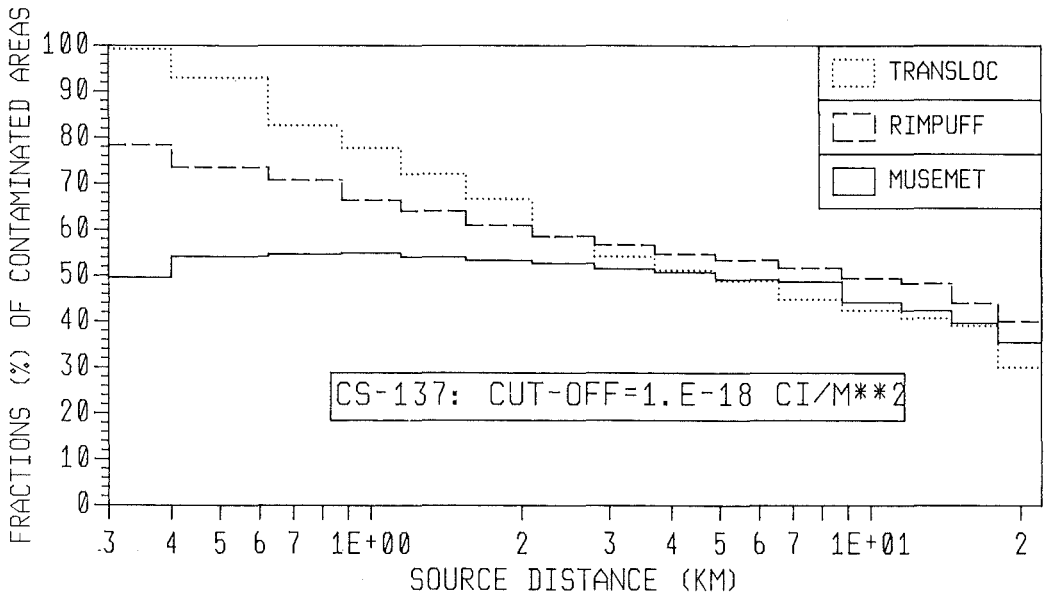

Figure 25. Mean relative size (%) of areas affected by different modelling concepts: nuclide considered: Cs-137

Two features are conspicuous:

1. Compared to the segmented plume model MUSEMET larger ares are affected by the puff model RIMPUFF in all distance bands. This could be expected because of the multiple puff modelling concept as it is explained schematically in Figure 7. Integrated from the source up to 20 km the difference between the mean areas contaminated by RIMPUFF and MUSEMET is about 10%. Because both models use the same meteorological data and the same set of diffusion parameters multiple puff modelling can be the only reason for this difference.

2. Very near to the source the areas affected by the numerical model are even larger (see Figure 25). Taking into account the low cut-off value, nearly 100% of the first distance ring are contaminated. This high percentage of course decreases if the cut-off value is increased, but the tendency still remains that TRANSLOC calculates significantly larger areas up to about one to two kilometres. One possible explanation might be numerical pseudo-diffusion. But it has been affirmed by the colleagues of the Battelle Institue and, therefore, it has been provided for the calculations, that numerical problems like pseudo-diffusion and instabilities, which might arise in TRANSLOC, are minimized or even avoided by the methods outlined briefly in Section 2.5. Thus, no other conceptual difference between the Gaussian-type models and the TRANSLOC version used in this study seems to be responsible for the result than the parametrization of diffusion by eddy diffusion coeffients.

To investigate this in some more detail three artificial Gaussian dispersion situations have been calculated with TRANSLOC: a very unstable one (Pasquill-Gifford category A), a neutral one (category D), and a stable on (category F). The constant meteorological conditions for each case are summarized in Table 19.

Category	u_0 (m/s)	$\partial T/\partial z$ (°K/100m)	K_z^{max} (m^2/s)	fitted diffusion coefficients	
				a	b
A	0.5	-2.0	70.6	65.1	0.41
D	3.0	-0.98	6.0	9.1	0.54
F	0.5	2.0	0.75	17.8	0.34

Table 19. TRANSLOC: Conditions for artificial Gaussian dispersion situations

In addition, the corresponding maximum of the vertical eddy diffusion coefficients, K_z which determine the horizontal diffusion coefficients (see Sect. 2.5) are indicated. The profiles of K_z calculated according to Eq. (2.12) are shown in Figure 26.

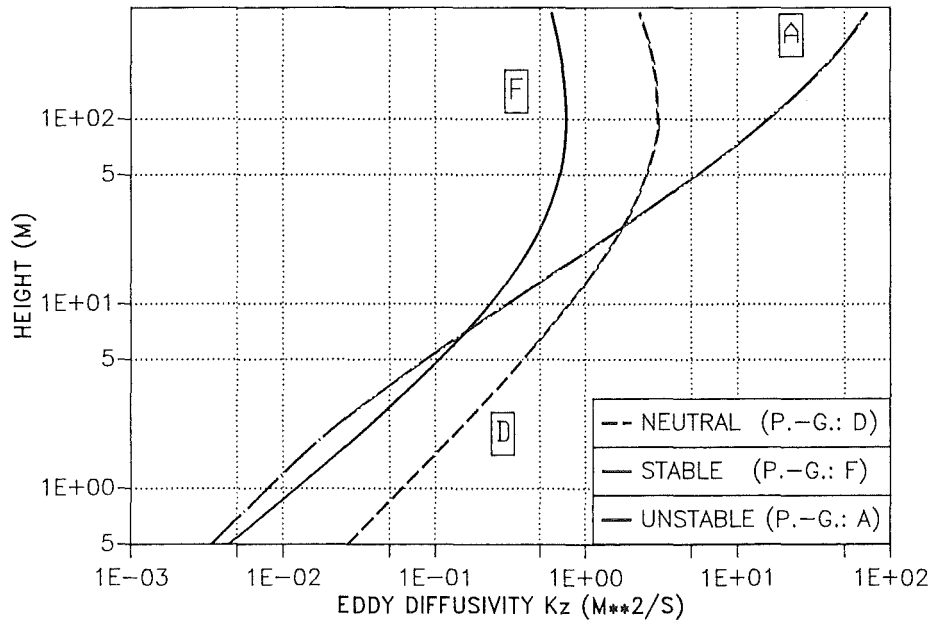

Figure 26. K-profiles corresponding to artificial Gaussian dispersion situations: (see Table 19)

To estimate the plume widths near to the ground in terms of the lateral Gaussian diffusion parameter $\sigma_y = \sigma_y(x)$, those lateral distances, y, normal to the plume's axis have been determined where the concentrations decreased to 1‰ of the values under the axis. Then σ_y can be calculated from the equation $y = \sigma_y \sqrt{2 \ln 1000} = 3.72\, \sigma_y$. Figure 27 shows the resulting σ_y-curves which have been fitted to a power function $\sigma_y = a\, x^b$ and compares them with the corresponding diffusion parameters used for MUSEMET and RIMPUFF which are determined from experiments (see also Table 2). The estimated diffusion coefficients a and b are also shown in Table 19.

Figure 27 depicts that over several hundred metres from the source the numerical model produces much broader plumes than the Gaussian-type models, a fact which has already been recognized during the deterministic comparative study, [10]. The reason for

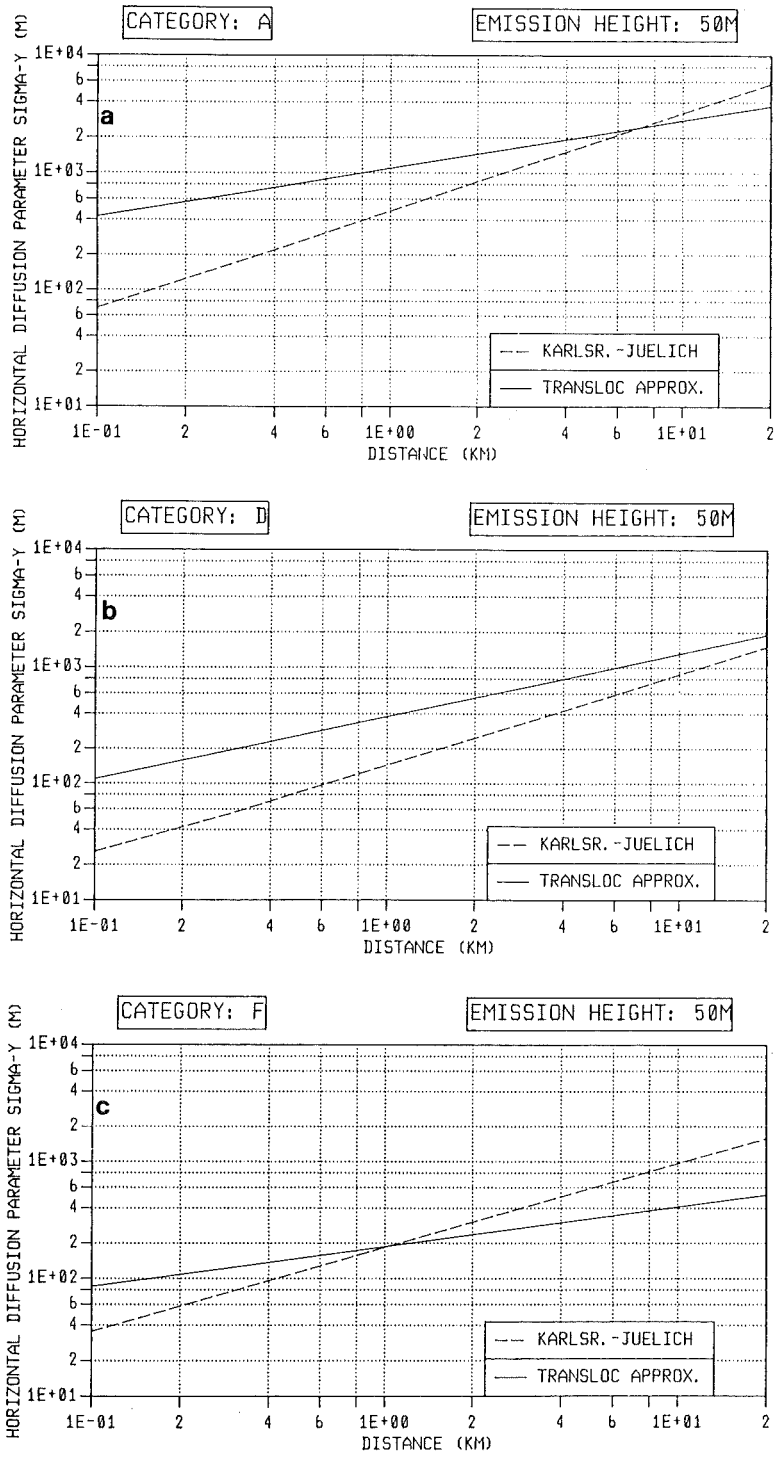

Figure 27. TRANSLOC: Artificial σ_y and corresponding Karlsruhe-Jülich parameters: a) category A, b) category D, c) category F

this is that the eddy diffusion coefficients implicitly comprise all scales of turbulent eddies which dominate the diffusion, also those whose size is larger than the size of a plume in the vicinity of the source. But this contradicts a basic assumption for the use of a numerical model, [18]. Therefore, its applicability in the first few hundred metres is questionable.

During the analyses of the TRANSLOC calculations possible inconsistencies between vertical temperature profiles and stability categories became apparent (Figure 28).

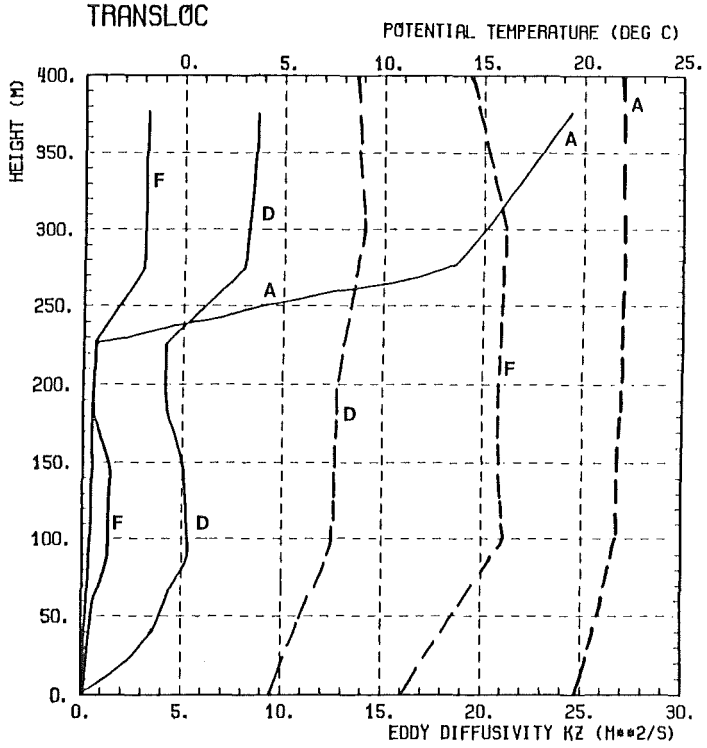

Figure 28. Possible relationship between temperature profiles, stability categories and K_z profiles in TRANSLOC:
broken line: potential temperature, upper scale
full line : eddy diffusivity, lower scale

The stability categories are needed to calculate the vertical wind profiles from surface observations of wind speed according to Eq. (2.7) because upper level wind data have not been available. They are derived according to the Klug-Manier typing scheme, [47], [48], using routine synoptic measurements, and converted to the Pasquill-Gifford categories (see Table 3). The temperature profiles have been derived by a simple averaging from radiosonde measurements which are carried out twice daily (12.00 UTC and 00.00 UTC) at the stations Essen and Stuttgart which are nearest to the chosen meteorological station Frankfurt/Airport (see Sect. 3.1). The averaged profiles of 12.00 UTC are assigned to the daytime from 6.00 a.m. to 6.00 p.m., the profiles obtained at midnight are used for the nighttime (7.00 p.m. to 5.00 a.m.), [45]. Figure 28 shows three specific profiles of potential temperature which are calculated from the corresponding temperature profiles available in the meteorological data set for the TRANSLOC calculations. In addition, the

Pasquill-Gifford stability classes derived for the same times are indicated. It is evident that in the cases shown, temperature profiles and stability classes do not match, except for the category F in the surface layer, and that the reliability of the corresponding K_z profiles, which are also shown in the Figure, is rather questionable. This should not be interpreted as a shortcoming of the specific numerical model TRANSLOC, but it should demonstrate, that a reliable use of a numerical model in general depends on the physical consistency of the meteorological data set. Because such data are generally not available from routine measurements in a sufficient quantity, they have to be derived from boundary-layer models using observations - an additional effort which is too high with respect to computing time in the context of ACAs.

Figure 29 shows the time-integrated air concentations near to the ground surface and the ground concentrations of Cs-137 in different distance ranges averaged over all weather sequences considered and over all azimuthal sectors in each distance band. They can be interpreted as the concentrations which are to be expected at any azimuthal position in the corresponding distance range.

The figures show that the concentrations related to RIMPUFF and MUSEMET are in very good agreement. The air concentrations of TRANSLOC (Figure 29a) are siginificantly smaller than those of the Gaussian type models in the first few hundred metres . One reason for this certainly is the enhanced horizontal dilution as it was demonstrated in Figure 27 but which seemed to be physically questionable. A second reason might be that the parametrization of vertical diffusion by an eddy diffusivity leads to a reduced vertical mixing compared to the modelling by sigma parameters; of course, this also depends on the specific sigma values chosen. This consideration is supported by the fact that the mean air concentrations calculated with TRANSLOC increase with source distance and reach their highest values between one and two kilometres. In contrast to the air concentrations the mean ground values are in fairly good agreement in all distances (Figure 29b). The difference between TRANSLOC and the other two models does not exceed a factor 1.5. The mean contributions to the ground contamination due to dry deposition show quantitatively the same differences as the mean air concentrations because they are caluclated according to Eq. (2.13). Thus, the alignment of ground concentrations is solely due to the contributions by wet deposition which are calculated according to Eq. (2.14). Near to the source the wet contribution of TRANSLOC is, on the average, larger because the depletion of the radioactive cloud due to dry deposition is smaller than for MUSEMET and RIMPUFF and more radioactive material is available to be deposited by rain. With increasing distance the amount of wet deposition contributing to the ground contamination slightly decreases so that, on the average, the ground concentration levels calculated with the numerical model become comparable to those of the Gaussian trajectory models.

Consistency between the three model types with respect to major transport directions of the radioactive material is demonstrated in Figure 30.

For Cs-137 it shows the azimuthal distributions of the average time-integrated air concentrations and of the average ground concentrations at source distances of 750m and 10km. The concentrations are averaged over all weather sequences and they are represented by their decadic logarithms. In the polar diagrams the angular direction is counted clockwise according to the wind rose. The figures confirm again the very good

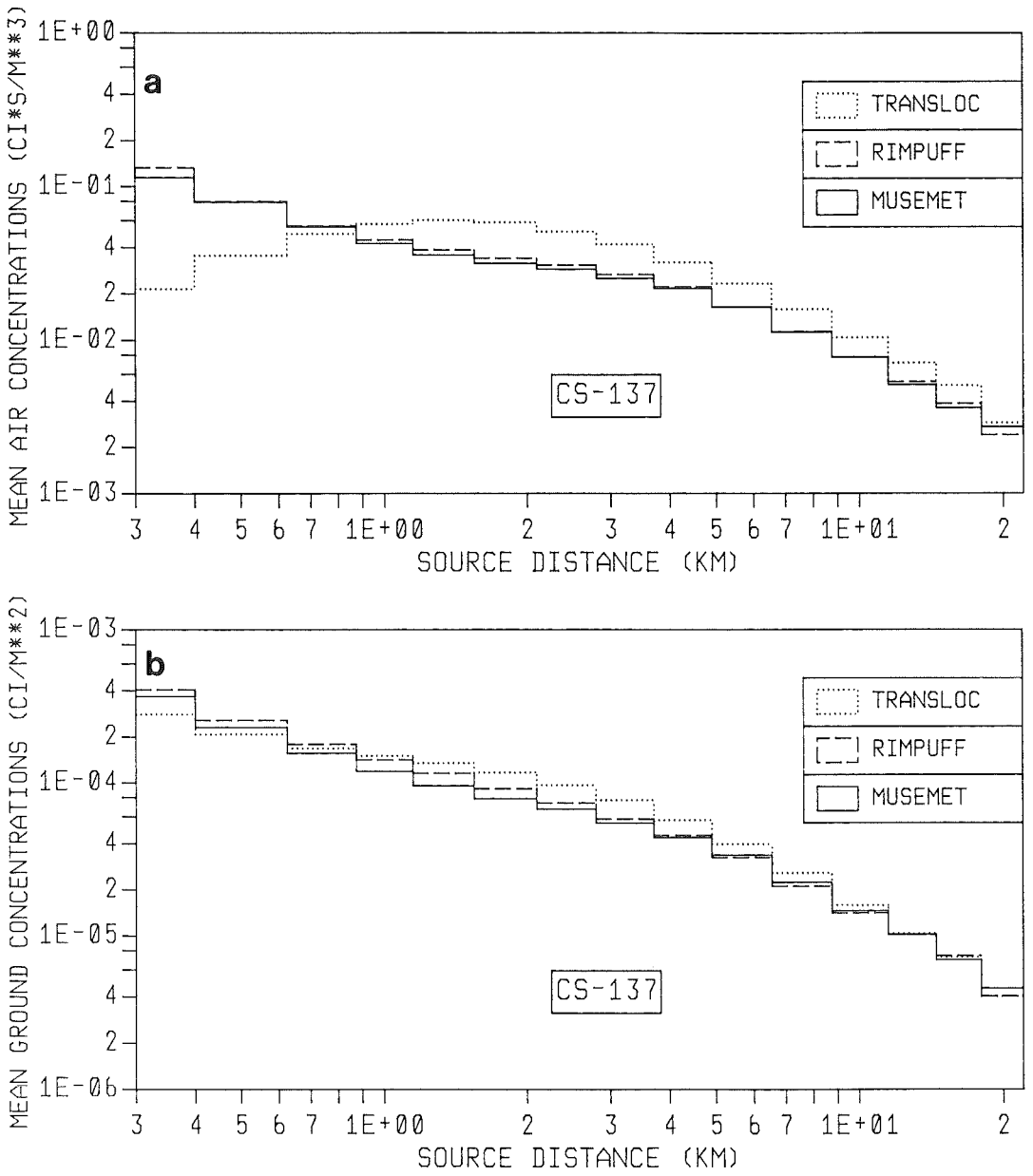

Figure 29. Mean concentrations of Cs-137 as functions of distance:
a) time-integrated air concentration
b) ground concentration

agreement between MUSEMET and RIMPUFF and the differences between these models and TRANSLOC.

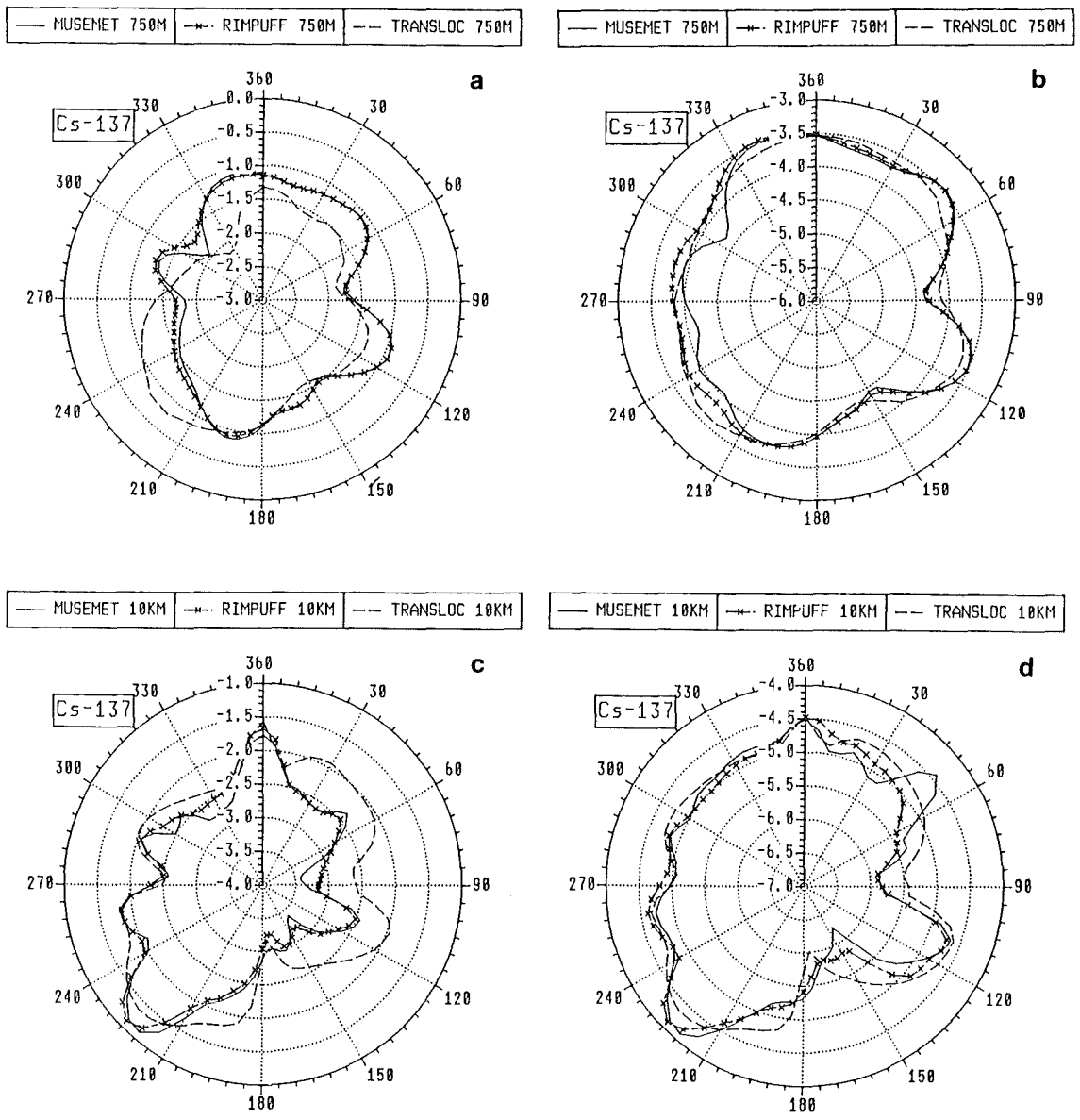

Figure 30. Azimuthal distributions of decadic logarithms of Cs-137 concentrations:
a) time-integrated air concentration, 750m b) ground concentration, 750m
c) time-integrated air concentration, 10km d) ground concentration, 10km

Consequences	MUSEMET	RIMPUFF	TRANSLOC
No. of late fatalities in living generation	185	186	262
No. of late fatalities in descendants	16	19	27
No. of late fatalities in all generations	201	204	289
Area B (km^2) (fast relocation)	0.06	0.09	0.01
No. of people affected by fast relocation	21	26	5
Area C (km^2) affected by relocation	6.3	5.7	5.8
No. of people relocated from area C	1720	1461	1386
Area D (km^2) affected by decontamination	66.2	73.5	96.8
Areas (km^2) with food-ban in the 1. year (all products)	594.6	685.4	736
Areas (km^2) with food-ban in the following years (all products)	85.2	90.9	113

Table 20. Mean values of accident consequences for different types of disperison models

Table 20 shows the mean (=expectation) values of accident consequences, except early fatalities, resulting from the application of MUSEMET, RIMPUFF, and TRANSLOC under the assumption that the COMP2 release occurred. Early fatalities do not appear because the 100 rem threshold is exceeded only inside the evacuation area A up to a source distance of 750m where, in addition, no people are living. Generally it can be stated, that the differences between the models are small but, however, some tendencies can be read off the table.

The size of area B and, thus, the number of people affected by fast relocation are smaller for the numerical model, indicating that the corresponding threshold for potential doses (Figure 9) is exceeded in less accident situations and smaller areas. The opposite trend can be observed for long-term countermeasures and the stochastic health effects. Low concentration and dose levels seem to be raised compared with the Gaussian-type models, so that the low intervention levels which determine the long-term protective actions are exceeded more often.

Comparing the results of benchmark task 1 (Sect. 4.1) and task 2 qualitatively, it is conspicuous that the differences in the accident consequences are going into the same direction if models, which are more complicated, are applied (trajectory versus straight-line Gaussian models, numerical versus Gaussian trajectory models). Consequences in the early phase after the artificial accidents considered in this study are reduced. Thus, the common opinion is valid that especially the straight-line Gaussian model leads to conservative assessments of non-stochastic consequences. But long-term consequences are underestimated if the simpler model is used and the conservatism arguement does not hold any longer.

Section 4.2 showed that under the assumptions of the COMP2 source term, single station meteorology, and homogeneous topography, the different concepts of Gaussian-like trajectory and numerical modelling lead to comparable results of the ACA. The restricted number of meteorological input parameters and possible physical inconsistencies in the data might cut the advantages of a numerical modelling and lead to non-reliable results for single cases. But with regard to ACAs, the Eulerian model can be applied succesfully. Thus, only the CPU-time, which is too high on a scalar processor (Table 17), excludes the numerical modelling concept from the application in ACAs.

4.3 Influence of inhomogeneous wind fields

The third benchmark task had been designed to study the influence of inhomogeneous meteorological fields on ACAs (see Sect. 3.3). It has been assumed that the COMP2 release occurred (see Sect. 3.2). The dispersion calculations have been performed with the RIMPUFF and the MUSEMET models. RIMPUFF used meteorological input data which varied in time and space. These data were available at eight stations located in a 200km circle around the source and they have to be transformed into data on a rectangular (x,y)-grid with a grid size of 20km*20km (Figure 14, Figure 31). Table 13 indicates that the fields of atmospheric stability and precipitation are mainly determined by the measurements at the four stations Frankfurt, Saarbrücken, Stuttgart, and Köln, and the two stations Frankfurt and Würzburg, respectively. Only the wind fields are derived from the measurements at the eight different stations (Figure 31).

The point data of wind speed, wind direction, and precipitation at the stations are converted to grid point values by an interpolation scheme using a $1/r^2$-weighting function where r represents the distance from a (x,y)-grid point to the measurement station. All stations lying in a 50km-radius around the grid point are considered by calculating a weighted sum; the radius is indicated in Figure 31 by the circle around the source site which is located in the middle of the area. If no station inside the circle is available only the data from that station are taken which is closest to the grid point; a weighting will not be performed.

The calculations with MUSEMET are based on single meteorological station data measured at Frankfurt/Airport.

Figure 32 and Figure 33 show examples of trajectories which are calculated by MUSEMET and RIMPUFF (only for the first puff) taking into account single meteorological wind data and inhomogeneous wind fields, respectively. Figure 32 demonstrates that

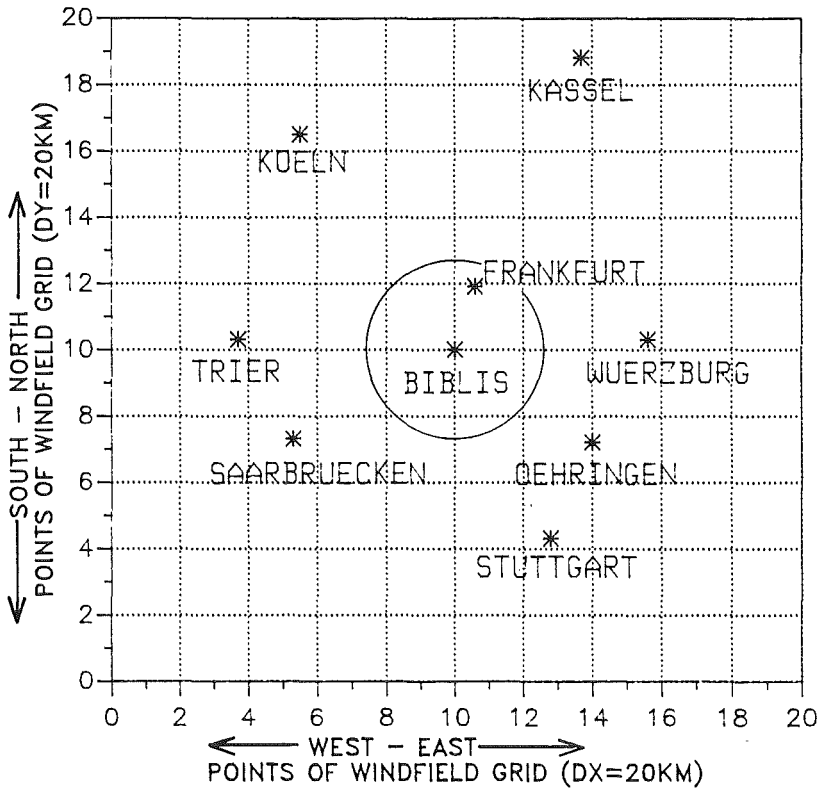

Figure 31. Rectangular grid of meteorological fields for RIMPUFF calculations ($\Delta x = \Delta y =$ 20km) and locations of meteorological stations inside the grid: the circle around the source indicates the 50km-interpolation radius

completely different trajectories can appear so that completely different regions are affected by the radioactive plumes. But also trajectories are possible which are in qualitative good agreement (Figure 33) so that the influence of inhomogeneous wind fields can be neglected.

The scatter diagram in Figure 34 compares for each weather sequence and each release phase of the COMP2 source term the travel times which the MUSEMET plumes need to leave the 200km-circle, with the times passed until the last puff tracked by RIMPUFF has left the area.

Generally, the application of the more complex model (RIMPUFF) with the consideration of inhomogeneous wind fields leads to longer residence times of the radioactive clouds over the dispersing area. There is a large scatter between five hours and 40 hours but even differences of 60 hours are possible. The conclusion that the longer residence times are due to the consideration of wind fields has been confirmed by a reference calculation with RIMPUFF which was based on the single meteorological station data of Frankfurt/Airport. In this case the correlation between the travelling times of MUSEMET and RIMPUFF was very good.

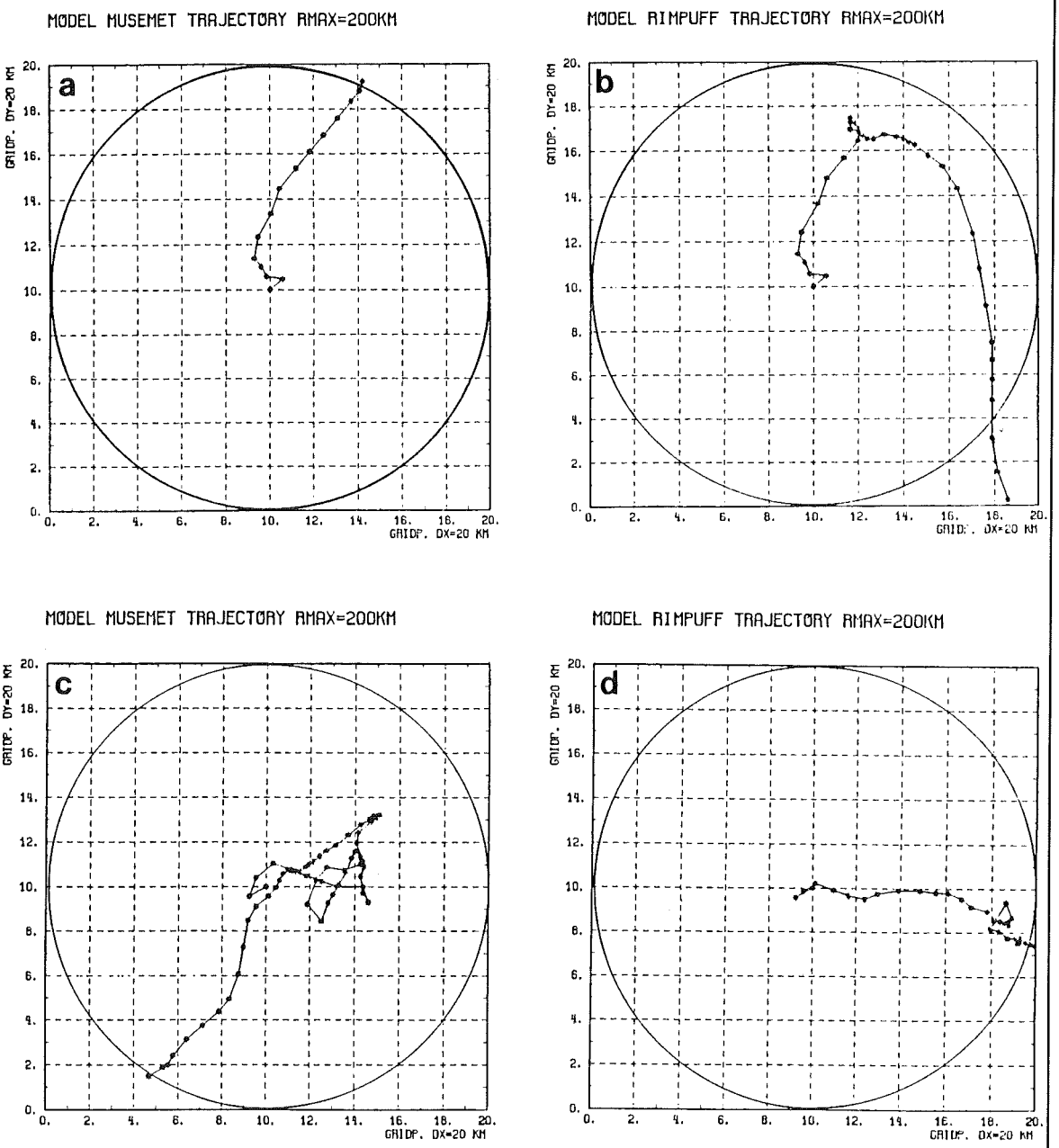

Figure 32. Examples of MUSEMET and RIMPUFF trajectories:
a) weather sequence 11, MUSEMET b) weather sequence 11, RIMPUFF
c) weather sequence 24, MUSEMET d) weather sequence 24, RIMPUFF

The agreement in the average time-integrated air and ground concentrations was nearly perfect if both models used the identical meteorological data (see also Sect. 4.2). Figure 35 shows that in the case of inhomogeneous wind fields taken into account by RIMPUFF the agreement is also rather good. The slightly higher ground, but lower air concentration values of RIMPUFF, which appear in nearly all distances, are a conse-

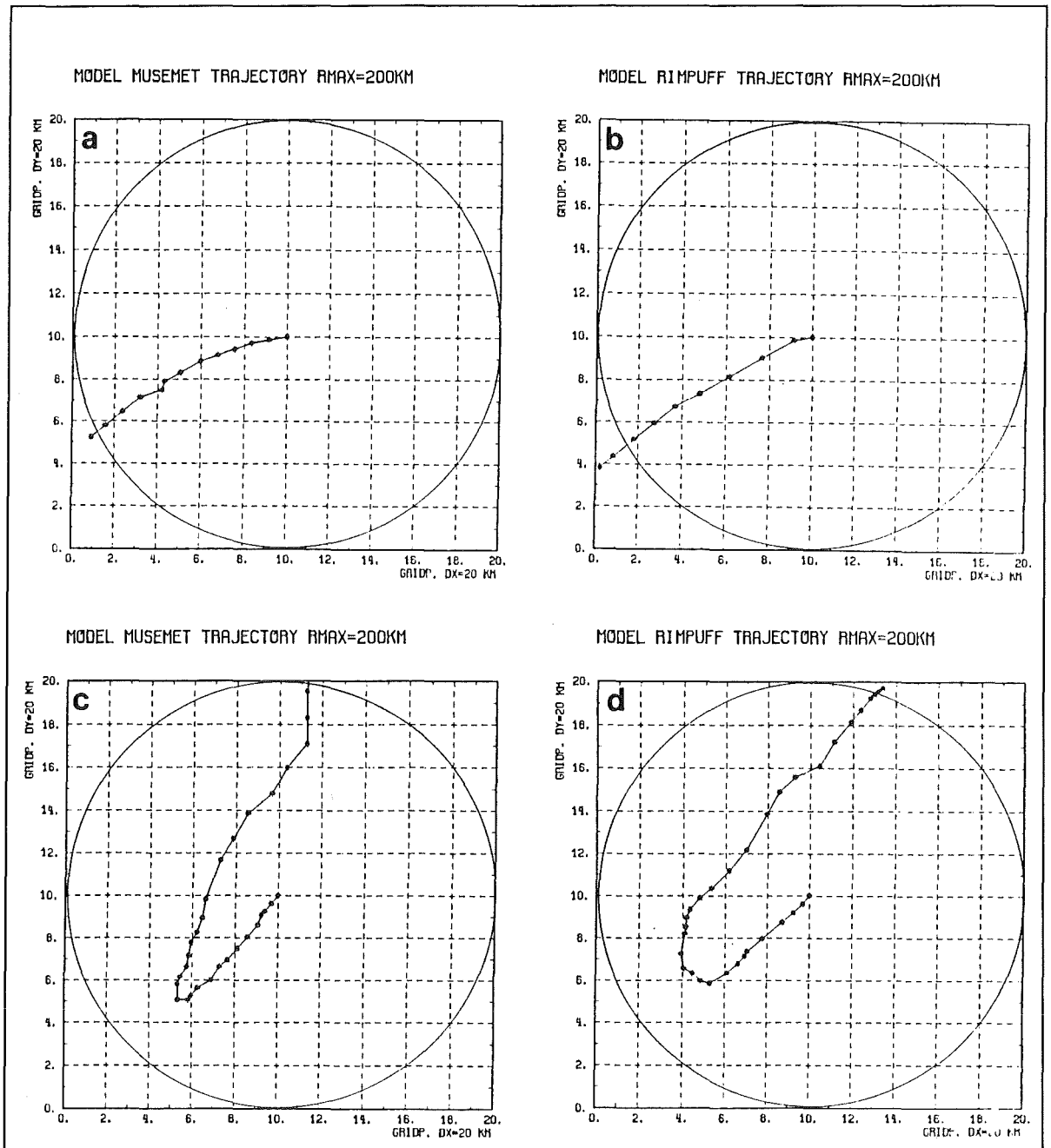

Figure 33. Examples of MUSEMET and RIMPUFF trajectories:
a) weather sequence 31, MUSEMET b) weather sequence 31, RIMPUFF
c) weather sequence 48, MUSEMET d) weather sequence 48, RIMPUFF

quence of the longer residence times of the radioactive material over the area, leading to enhanced deposition on the ground but also to a stronger depletion of the clouds.

Figure 36 indicates the spatial distribution of ground concentrations of Cs-137 above a cut-off value of $C^{gr}_{cut} = 10^{-18}$ (Ci m^{-2}) for the calculation without wind fields (MUSEMET, full

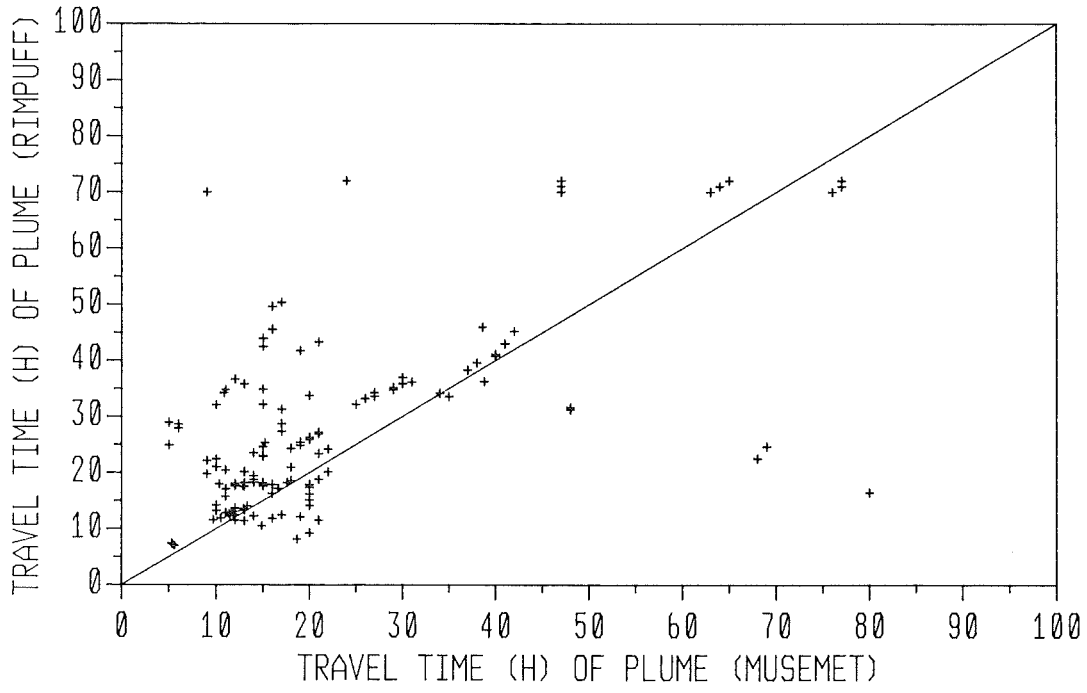

Figure 34. Travelling times (h) of MUSEMET plumes and RIMPUFF puffs to leave a 200km-circle around the source

line), with wind fields (RIMPUFF, dashed line) as well as for the RIMPUFF reference calculation with the same data as MUSEMET (dotted line).

The result that smaller areas are affected by the puff model RIMPUFF is in contrast to the result of benchmark task two where it was concluded that the puff modelling concept leads to larger contaminated areas. From the reference calculation with RIMPUFF and from the schematic illustration in Figure 37 the conclusion can be drawn that the puff modelling concept as well as the use of different meteorological data bases are responsible for the differences shown in Figure 36. Figure 37 depicts a part of a polar grid system. A possible straight-line trajectory segment during an n-th time interval is represented by the thick, full line. A sequence of puffs is advected and dispersed downwind according to the meteorological conditions prevailing during the time interval. According to the concept of MUSEMET, a rectangular (ξ_n, η_n) -coordinate system is also shown with its origin in the starting point of the trajectory segment and ξ_n directed downwind.

As it is sketched in the diagram only those gird points lying inside the horizontal circular puff areas are affected by RIMPUFF. The finite extensions of the puff areas are defined by the radii of influence, r_p . With respect to MUSEMET also those grid points outside the circular puff regions, but with positive ξ_n -coordinates which are less or equal to the length of the n-th trajectory segment are considered. Especially in farther source distances the density of the polar grid points is rather small and less points lie inside the

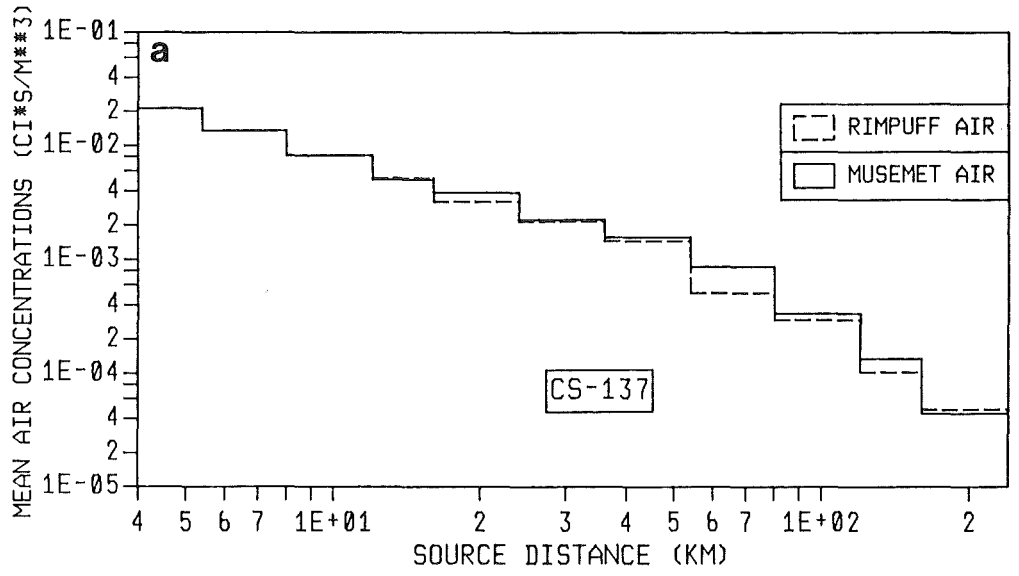

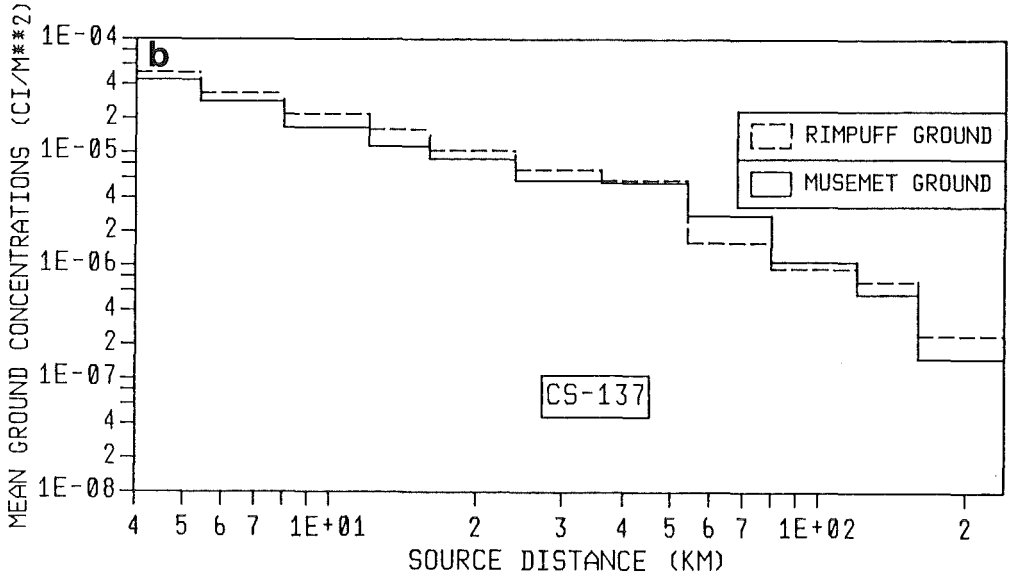

Figure 35. Mean concentrations of Cs-137 as functions of distance:
a) time-integrated air concentration
b) ground concentration

limited puff areas, so that the difference in the number of grid points which are affected by MUSEMET and RIMPUFF increases. On the other hand, the calculations have been carried out with puff radii of $r_p(x) = 6\,\sigma_y(x)$. Therefore, with respect to the Gaussian distribution of concentrations much more than 99.9% of all possible values have been considered ($r_p = 3.29\,\sigma_y$ corresponds to 99.9%). From this point of view the contamination of smaller areas using RIMPUFF seems to be more realistic, particularly as the contamination outside the puff areas does not contribute at all to the average concentration distribution. Comparing the results of the two RIMPUFF calculations demonstrates that the

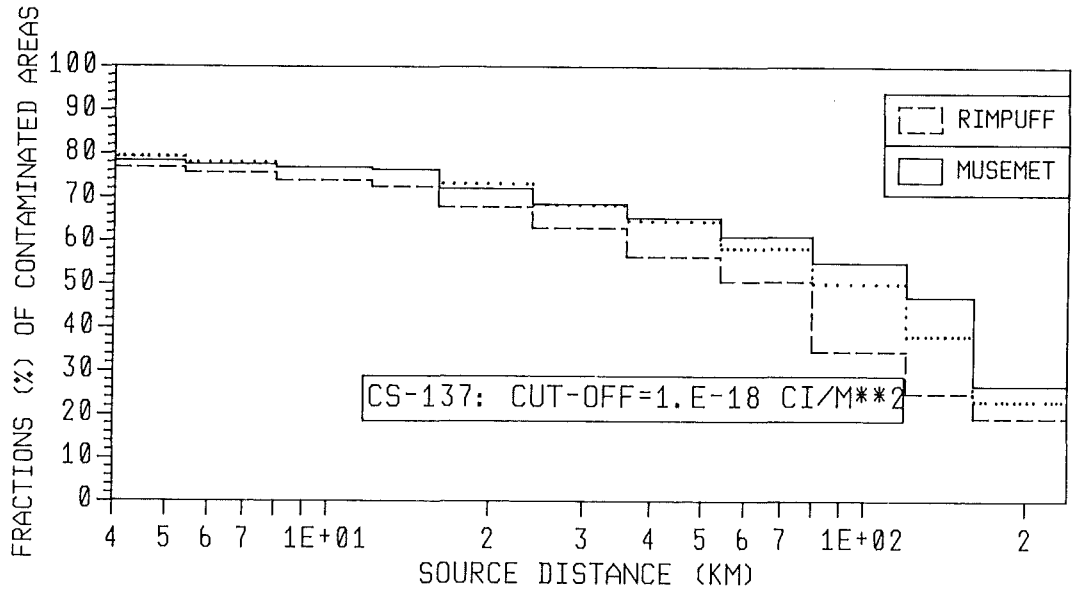

Figure 36. Mean relative size (%) of contaminated areas: nuclide considered: Cs-137
full line: MUSEMET
dashed line: RIMPUFF with wind fields
dotted line: RIMPUFF without wind fields

consideration of more realistic atmospheric conditions even enlarge the difference between the puff model and the segmented plume model.

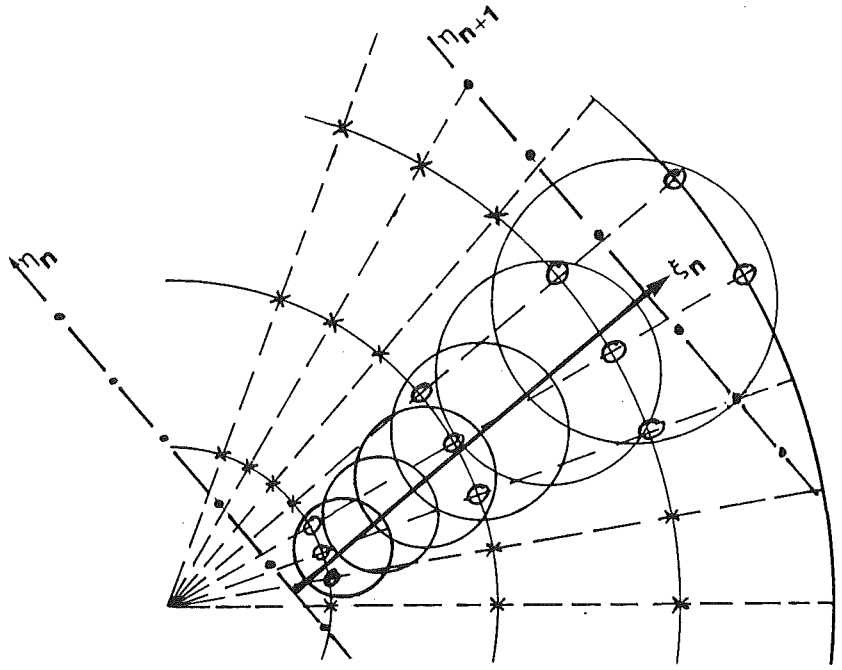

Figure 37. Illustration of contributions of RIMPUFF and MUSEMET to the contamination at polar grid points: (further explanations see text)

Consequences	MUSEMET	RIMPUFF, with wind fields
No. of late fatalities in living generation	2312	2298
No. of late fatalities in descendants	367	390
No. of late fatalities in all generations	2679	2688
Area B (km^2) (fast relocation)	0.04	0.02
No. of people affected by fast relocation	14	5
Area C (km^2) affected by relocation	7.3	5.9
No. of people relocated from area C	2473	1883
Area D (km^2) affected by decontamination	446.1	593.8
Areas (km^2) with food-ban in the 1. year (all products)	35026	24145
Areas (km^2) with food-ban in the following years (all products)	477.2	621.3

Table 21. Mean values of accident consequences for different Gaussian disperison concepts

Table 21 summarizes the mean values of accident consequences resulting from the application of MUSEMET and RIMPUFF on the basis of homogeneous and inhomogeneous meteorological data, respectively. It has been assumed that the COMP2 release occurred. As in Sect. 4.2 it can be stated that the differences between the models are rather small. Neglecting the very small absolute values of the mean number of persons and the size of areas which are affected by fast relocation, the largest differences appear for the areas affected by food-bans and decontamination. But all these differences are smaller than a factor of 1.5. The numbers of late fatalities agree within 1%.

There is some indication in the results that the application of wind fields leads to a reduction of high concentration and dose levels, as it was already sketched in Figure 21, and thus, to a reduction of those countermeasures which depend on a relatively high dose intervention threshold like fast relocation out of area B. On contrast, protective actions depending on low intervention levels like food-bans in the following

years and decontamination are taken in larger areas. Since decontamination and relocation are not independent (if land areas can be decontaminated effectively, there is no need to relocate the inhabitants), the size of area C and the number of people relocated are smaller. Only the size of areas which are affected by food-bans during the first year after the accident seems not to match with this argumentation. But Figure 36 showed that the radioactive materials were deposited over larger areas if the model MUSEMET was applied. And because the threshold to interdict the consumption of foodstuffs just after the accident is very low [2], it is exceeded very easily over rather large areas.

5. SUMMARY AND CONCLUSION

It was the essential aim of the study to identify improved atmospheric dispersion models which can be applied in ACA codes as a substitute of the conventional straight-line Gaussian plume model. Additionally, it was tried to give quantitative indications of the implications which different types of atmospheric dispersion models might have on the results of ACAs. Furthermore, attention was directed on the availability of meteorological input data and the computer time spent by the models. It is necessary in ACAs that the atmospheric dispersion model can be applied with reasonable computer time. Additionally, it has to be devised with the requirement that it uses real meteorological data extracted from routine observations which are recorded and reported continuously from meteorological stations. The only data needed by Gaussian-like models are measurements of wind speed, wind direction, and precipitation intensity, and, in addition, the stability class which can be derived from synoptic observations.

For these purposes probabilistic comparative calculations have been performed with different kinds of atmospheric dispersion models on the basis of artifical source terms. The model types were:

- a conventional straight-line Gaussian plume model which does not take into account any information on the wind direction;
- a straight-line Gaussian plume model which consideres only the real wind direction at the beginning of hourly release phases;
- a segmented plume model which is a special kind of a Gaussian-like trajectory model taking into account hourly changes of spatially homogeneous meteorological conditions during the release and the dispersion (MUSEMET, [11]);
- a Gaussian-like trajectory puff model which is able to consider meteorological data which change temporally and spatially (RIMPUFF, [12]);
- a Eulerian grid-point model which solves Eq. (2.1) numerically and which is potentially able to consider explicitly the three-dimensional inhomogeneous and instationary wind- and turbulence fields in the atmosphere; unfortunately, the necessary meteorological input data which should also comprise vertical profiles of temperature and wind to assess the vertical turbulent diffusion have not been available with the required quantity, so that necessary approximations also reduced their quality (TRANSLOC, [13]).

The main result of the study is that there are Gaussian-like trajectory models available to substitue the straight-line Gaussian model in ACAs. The demands for availability of meteorological data and reasonable computer time are fulfilled by the segmented plume model as well as by the puff model, but with the restriction that for running the puff model a vector processor should be used. The principal reason why the numerical modelling concept has to be excluded from the application in ACAs is the CPU-time which is very much to high on a scalar computer and it can be assumed that also the use of a vector processor would not reduce this time to acceptable absolute values. With respect to the probabilistic results of an ACA the Eulerian model could also be applied successfully, although the restricted number of meteorological input parameters which were available and physical inconsistencies in these data might have cut the physical advantages of a numerical modelling and lead to non-reliable results for single cases.

Under the assumptions of the source terms considered in this study and dependent on their characteristics, quantitative differences which were more or less pronounced arose in the accident consequences due to the application of different atmospheric dispersion models. The study showed that using a trajectory model leads to

- a spatial distribution of activity over larger areas;
- an increase of radioactive plume's residence time in the area over which it is dispersing ;
- enhanced depletion and dilution by dry and wet deposition processes and turbulent diffusion along the longer trajectories.

On the basis of the source terms considered, the comparative calculations indicated that the consequences in the early phase after the accident are reduced applying a Gaussian-like trajectory or even more complex models. Thus, the straight-line Gaussian model may give conservative results in the assessment of early health effects. But long-term consequences and countermeasures are underestimated if the simpler model is used and the conservatism argument does not hold any longer.

Generally, it can be stated that the application of trajectory models provides more realistic results of ACAs than the straight-line models because the condsideration of changes of wind direction gives a more realistic picture of the atmospheric conditions. There are no stringent arguments to apply only a straight-line Gaussian model in ACAs. This comparative study showed clearly that Gaussian-like trajectory model are as easy to apply as the straight-line plume model. Regardless whether the differences between the trajectory and the straight-line model are larger or smaller than a factor of two for a certain source term, the acceptance of the results of an ACA will increase if the improved model is used. Furthermore, the applicability of ACA codes will increase from the comprehensive and realistic assessments of consequences towards a powerful tool in a decision-making framework (e.g. emergency planning, siting, research priority setting).

UFOMOD	
Near range model ($\leq$ 50km)	Far range model ($\geq$ 50km)
Atmospheric dispersion	
MUSEMET (KFA) RIMPUFF (RISO)	MESOS (ICST) Wind fields in the region 10°W - 50°E, 36°N - 62°N
synoptic data recorded and reported continuously at 1h intervals	synoptic data of 1982 and 1983 reported from more than 800 measuring stations at 3h intervals

Figure 38. UFOMOD: Modelling of atmospheric dispersion: (adapted from [57])

Therefore, it was a logical consequence from this study to apply trajectory models in the new program system UFOMOD [57] for assessing the consequences of nuclear acci-

dents. This led to a completely novel concept of atmospheric dispersion modelling in the new UFOMOD (Figure 38). Due to the facts, that

- site-specific characteristics are only relevant in the near range and vanish at farther distances,
- the quality and quantity of consequences in the near range (fast protective measures, early health effects) are different from the far range (long-term countermeasures, stochastic health effects),
- the near range can be modelled much more in detail than the far range,
- many applications of ACA refer to only one of both distance ranges

different ranges of validity are distinguished and assigned to respective trajectory models:

- the near range ($\leq$ 50 km), where modified versions of the atmospheric dispersion models MUSEMET and RIMPUFF are used;
- the far range ($\geq$ 50 km), where the computer code MESOS is applied [59]. It is a long-range dispersion model simulating the transport of radioactive material over large areas up to thousands of kilometres. It combines the requirement of short computing time with the ability to disperse radioactive material along precalculated wind fields derived from synoptic meteorological data measured within whole Europe.

More detailed descriptions of the new concept and the modified atmospheric dispersion models can be found in [57] and [58].

ACKNOWLEDGMENTS

The author whishs to thank all members of the ACA-Group of the Institut für Neutronenphysik und Reaktortechnik at the Kernforschungszentrum Karlsruhe for many discussions helping to perform this study. Mr. W. Raskob from the Dr. Trippe Ingenieurbüro, Karlsruhe, assisted to modify the RIMPUFF model and performed most parts of the calculations with respect to RIMPUFF and TRANSLOC. Especially, I have to thank Dr. J. Ehrhardt who patiently helped me to find the right way through the maze of UFOMOD results.

6. REFERENCES

[1] Bundesminister für Forschung und Technologie (Hrsg.)
Deutsche Risikostudie Kernkraftwerke - Eine Untersuchung zu dem durch Störfälle in Kernkraftwerken verursachten Risiko
Fachband 8: Unfallfolgenrechnung und Risikoergebnisse.
Verlag TÜV Rheinland GmbH, Köln, 1981

[2] Bayer, A., K. Burkart, J.Ehrhardt, W. Hübschmann, M. Schückler, S.Vogt, W. Jacobi, H.G.Paretzke, K.-R.Trott, E.Hofer and B.Krzykacz
The German Risk Study: Accident Consequence Model and Results of the Study
Nuclear Safety, 59, 20-50, 1982

[3] International Atomic Energy Agency
Atmosperic Dispersion in Nuclear Power Plant Siting: A Safety Guide
IAEA, Vienna, 1980, STI/PUB/549

[4] Pasquill, F. and F.B. Smith
Atmospheric Diffusion
3. Edition
Ellis Horwood Ltd., Chichester, U.K., 1983

[5] Rasmussen, N.C.
Reactor Safety Study. An Assessment of Accident Risks in U.S. Commercial Nuclear Power Plants
(NUREG-75/014), WASH-1400. U.S. Nuclear Regulatory Commission, Washington, D.C., October 1975

[6] Ritchie, L.T., J.D. Johnson and R.M. Blond
Calculations of Reactor Consequences, Version 2
Sandia National Laboratories, SAND81-1994, (NUREG/CR-2324), 1981

[7] Clarke, R.H. and G.N. Kelly
MARC - The NRPB Methodology for Assessing Radiological Consequences of Accidental Releases of Activity
National Radiological Protection Board, UK - Chilton, Didcot, NRPB-R127, 1981.

[8] Ritchie, L.T., D.I. Chanin and J.L. Sprung
MELCOR Accident Consequence Code System (MACCS), Volume II
MACCS Reference Manual
Sandia National Laboratories, SAND86-1562, (NUREG/CR-4691), 1987

[9] Hanna, S.R., G.A. Briggs and R.P. Hosker
Handbook on Atmospheric Diffusion.
Technical Information Center, U.S. Departement of Energy
Springfield, Virginia 22 161, U.S.A., 1982

[10] Päsler-Sauer, J.
Comparative Calculations and Validation Studies with Atmospheric Dispersion Models
KfK - 4164, Kernforschungszentrum Karlsruhe, 1986

[11] Straka, J., H. Geiss and K.J. Vogt
Diffusion of Waste Air Puffs and Plumes under Changing Weather Conditions
Contr.Atmosph.Physics, 54, 207-221, 1981

[12] Mikkelsen, T., S.E. Larsen and S. Thykier-Nielsen
Description of the RISOE Puff Diffusion Model
Nuclear Technology, 67, 56-65, 1984

[13] Hartwig, S. und G. Schnatz
TRANSLOC, ein numerisches Modell zur Simulation von Dispersionsvorgängen in der Atmosphäre und seine Anwendung für die Ausbreitung radioaktiver Substanzen bei einem Reaktorunfall.
Seminar on Radioactive Releases and their Dispersion in the Atmosphere Following a Hypothetical Reactor Accident, RISOE, 22.-25.4.1980, Vol.2, 555-574
Commission of the European Communities, Luxembourg, 1980

[14] McNaughton, D.J., D.C. Powell
RAPT - The Pacific Northwest Laboratory Air Pollution Transport Model: A Guide
PNL - 3390. UC - 11, 1980

[15] Kao, S.K.
Theories of Atmospheric Transport and Diffusion
in: [16], Chap. 6, 189-239, 1984

[16] Randerson, D. (Editor)
Atmospheric Science and Power Production
DE84005177 (DOE/TIC-27601)
National Technical Information Center, 1984
U.S. Department of Commerce
Springfield, Virginia 22 161

[17] Sutton, O.G.
Micrometeorology
McGraw-Hill Book Company, New York, 1953, pp. 333

[18] Hanna, S.R.
Turbulent Diffusion: Chimneys and Cooling Towers
Chapter 10 in: Plate, E. (Editor)
Engineering Meteorology
Elsevier Publishing Company, Amsterdam - Oxford - New York, 1982

[19] Der Bundesminister der Justiz (Hrsg.)
Bekanntmachung der Leitlinien zur Beurteilung der Auslegung von Kernkraftwerken mit Druckwasserreaktoren gegen Störfälle im Sinne des § 28 Abs. 3 der Strahlenschutzverordnung --- Störfall-Leitlinien ---
Bundesanzeiger, Jahrgang 35, Nummer 245a, 1983,
Der Bundesminister der Justiz, 5300 Bonn, FRG

[20] Thomas, P., W. Hübschmann, L.A. König, H. Schüttelkopf, S. Vogt and M. Winter
Experimental Determination of the Atmospheric Dispersion Parameters over Rough Terrain
Part 1: Measurements at the Karlsruhe Nuclear Research Center
KfK - 2285, Kernforschungszentrum Karlsruhe, 1976

[21] Thomas, P., K. Nester
Experimental Determination of the Atmospheric Dispersion Parameters over Rough Terrain
Part 2: Evaluation of Measurements
KfK - 2286, Kernforschungszentrum Karlsruhe, 1976

[22] Thomas, P., H. Dilger, W. Hübschmann, H. Schüttelkopf and S. Vogt
Experimental Determination of the Atmospheric Dispersion Parameters at the Karlsruhe Nuclear Research Center for 60m and 100m Emission Heights
Part 1: Measured Data
KfK - 3090, Kernforschungszentrum Karlsruhe, 1981

[23] Thomas, P., K. Nester
Experimental Determination of the Atmospheric Dispersion Parameters at the Karlsruhe Nuclear Research Center for 60m and 100m Emission Heights
Part 2: Evaluation of Measurements
KfK - 3091, Kernforschungszentrum Karlsruhe, 1981

[24] Geiß, H., K. Nester, P. Thomas und K.J. Vogt
In der Bundesrepublik Deutschland experimentell ermittelte Ausbreitungsparameter für 100 m Emissionshöhe
Jül - 1707, KfK - 3095, Februar 1981
Kernforschungsanlage Jülich in Zusammenarbeit mit dem Kernforschungszentrum Karlsruhe

[25] Gifford, F.A.
Turbulent Diffusion-Typing Schemes: A Review
Nuclear Safety, 17, 68-86, 1976

[26] Ehrhardt, J. und S. Vogt
Unfallfolgenrechnungen und Risikoabschätzungen für Druckwasserreaktoren mit dem Rechenprogramm UFOMOD/B3
KfK - 3373, Kernforschungszentrum Karlsruhe, 1983

[27] Geiß, H.
Ein Verfahren zur realistischen Ermittlung der Umgebungsbelastung nach kerntechnischen Störfällen unter Einbeziehung von Meßwerten der Umgebungsüberwachung
in: Henning, K. (Redaktion)
Strahlenexposition der Bevölkerung
18. Jahrestagung des Fachverbandes für Strahlenschutz e.V.
6.-10. Oktober 1985 in Lübeck-Travemünde, FS-85-37-T

[28] Vogt, K.J., H. Geiß and J. Straka
A New Trajectory Model and its Application for Accident and Risk Assessments
12-th NATO/CCMS International Technical Meeting on Air Pollution Modeling and its Application, Palo Alto, 25./28.08.1981

[29] Start, G.E. and L.L. Wendell
Regional Effluent Dispersion Calculations Considering Spatial and Temporal Meteorological Variations
National Oceanic and Atmospheric Administration (NOAA) Technical Memorandum ERL-ARL-44, 1974

[30] Mikkelsen, T. and S. Thykier-Nielsen
Atmosperic Dispersion over Complex Terrain
in: Pearce, R.P. (Editor)
Proceedings of Workshop on Mesoscale Modelling, Turbulence and Diffusion, RISOE National Laboratory, Denmark, 12-15 May 1987, 103-110,
US Army Atmospheric Sciences Laboratory
White Sands Missile Range, New Mexico, 1987

[31] Mikkelsen, T., S.E Larsen and I. Troen
Use of a Puff Model to Calculate Dispersion from a Strongly Time Dependent Source
Seminar on Radioactive Releases and their Dispersion in the Atmosphere Following a Hypothetical Reactor Accident, RISOE, 22.-25.4.1980, Vol.2, 575-614
Commission of the European Communities, Luxembourg, 1980

[32] Mikkelsen, T., S.E Larsen and H.L. Pesceli
Diffusion of Gaussian Puffs
Q.J.R. Meteorol. Soc., 113, 81-105, 1987

[33] Commission of the European Communities
Methods for Assessing the Off-Site Consequences of Nuclear Accidents
Joint report by the Kernforschungszentrum Karlsruhe GmbH, D-Karlsruhe, and the National Radiological Protection Board, UK-Chilton, Didcot
CEC-Report EUR 10243 EN (1986)

[34] Yanenko, N.N
The Method of Fractional Steps
Springer Verlag, Heidelberg, 1971

[35] Richtmeyer, R.D. and K.W. Morton
Difference Methods for Initial Value Problems
Interscience Publication, New York, 1967

[36] Martens, R., K. Maßmeyer, W. Pfeffer, G. Haider und G. Morlock
Bestandsaufnahme und Bewertung der derzeit genutzten atmosphärischen Ausbreitungsmodelle
Bericht der Gesellschaft für Reaktorsicherheit mbH, Köln, 1987

[37] Haltiner, G.J.
Numerical Weather Prediction
John Wiley & Sons, Inc., New York, London, Sydney, Toronto, 1971

[38] Wu, S.S.
A Study of Heat Transfer Coefficients in the Lowest 400 Meters of the Atmosphere
Journ. Geophys. Res., 70, 1801-1807, 1965

[39] Schnatz, G.
private communication, Battelle Institut e.V., Frankfurt/Main April 1989

[40] Turner, J.S.
Buoyancy Effects in Fluids
Cambridge University Press, 1973

[41] Schwarz, G.
Deposition and Post-Deposition Radionuclide Behaviour in Urban Environments
in: Proceedings of Workshop on Methods for Assessing the Off-Site Radiological Consequences of Nuclear Accidents, 15-19 April 1985, Luxembourg, 533-557
Commission of the European Communities, Report EUR 10397 EN, 1986

[42] Vogt, S., W. Hübschmann und P. Wittek
Niederschlag und Washout im Unfallfolgenmodell der Deutschen Risikostudie - Kernkraftwerke
KfK - 3548, Kernforschungszentrum Karlsruhe, 1983

[43] Päsler-Sauer, J.
private communication, March 1985

[44] Turner, D.B.
Workbook of Atmospheric Dispersion Estimates
U.S. Department of Health, Education and Welfare, Public Health Service, Publ. No. 999-AP-26, 1969

[45] Rohbock, E. und G. Schnatz
Deutsche Risikostudie Kernkraftwerke Phase B
AP 16-2: Empfindlichkeitsanalyse zu den Ausbreitungsrechnungen
Abschlußbericht an die Gesellschaft für Reaktorsicherheit,
Blev-R-65080, Battelle Institut e.V., Frankfurt, April 1987

[46] Thykier-Nielsen, S. and S.E. Larsen
Benefits of the Use of Complex Dispersion Models in Accident Consequence Assessments with Special Emphasis on Emergency Planning
RISOE National Laboratory, Final Report on CEC-Contract 85E1009, 1986

[47] Klug, W.
Ein Verfahren zur Bestimmung von Ausbreitungskategorien aus synoptischen Beobachtungen
Staub, 29, 143, 1968

[48] Manier, G.
Vergleich zwischen Ausbreitungsklassen und Temperaturgradient
Meteorologische Rundschau, 28, 6-11, 1975

[49] Möllmann, M.
private communication, KFA Jülich, March 1985

[50] Friederichs, H.-G. und E. Schrödl
Neue Erkenntnisse zur Spaltproduktfreisetzung aus dem Kern und Reaktorgebäude bei Unfällen
Ergebnisse neuerer Sicherheitsanalysen, 10. GRS-Fachgespräch, Köln, 12.-13. November 1986, GRS 64, März 1987

[51] Gesellschaft für Reaktorsicherheit (GRS) mbH
Deutsche Risikostudie Kernkraftwerke Phase B
Eine zusammenfassende Darstellung
GRS-72, Köln, 1989

[52] Druwe, H.
private communication, Gesellschaft für Reaktorsicherheit (GRS) mbH, Köln, 1987

[53] Panitz, H.-J. and W. Raskob
private communication, 1987

[54] Geiß, H.
private communication, KFA Jülich, 1985

[55] Möllmann, M.
private communication, KFA Jülich, 1986

[56] Nester, K.
private communication, KfK, 1986

[57] Burkart, K., J. Ehrhardt, I. Hasemann, C. Matzerath, H.-J. Panitz and C. Steinhauer
The Program System UFOMOD for Assessing the Consequences of Nuclear Accidents
KfK - 4330, Kernforschungszentrum Karlsruhe, 1988

[58] Panitz, H.-J., C. Matzerath and J. Päsler-Sauer
UFOMOD: Atmospheric Dispersion and Deposition
KfK - 4332, Kernforschungszentrum Karlsruhe, 1989

[59] ApSimon, H.M., A.J.H. Goddard and J. Wrigley
Long-Range Atmospheric Dispersion of Radioisotopes - I. The MESOS Model
Atmospheric Environment, 19, 99-111, 1985